Synthesis and Characterization of Electrospun Activated Carbon Nanofibers Reinforced with Cellulose Nanocrystals for Adsorption Applications

by

Rania Awad

A thesis submitted in partial fulfillment of the requirements for the degree of

Master of Science
in
Environmental Science

Department of Civil and Environmental Engineering
University of Alberta

Abstract

Cellulose nanocrystals (CNCs) are emerging nanomaterials with desirable characteristics including biodegradability, renewable sources, high aspect ratios, high surface area, and high strength. Polyacrylonitrile (PAN) is the most commonly used polymer precursor for electrospinning due to its high melting point and large carbon yield. In this study, PAN/CNC nanofibers were electrospun from solutions of PAN and CNCs in N,N-dimethylformamide and were assessed for their adsorption performance. First, electrospinning conditions were optimized to form PAN-CNC composite nanofibers with uniform diameters and smooth morphology at CNC loadings of 0, 10, 20, and 30 % W_{CNC}/W_{PAN}. Second, electrospun PAN-CNC composite nanofibers were stabilized and then activated at 800°C with KOH as activating agent to produce activated carbon nanofibers (ACnFs). The ACnFs were then characterized for their morphological, thermal, mechanical, chemical properties, as well as their surface area and pore size distribution. Last, the adsorption properties of ACnFs were tested for methyl ethyl ketone (MEK) and cyclohexane. MEK and cyclohexane were selected because they are widely used organic solvents for industrial processes, and have similar boiling point, density and heats of vaporization (similar heats of adsorption).

Scanning electron microscopy images revealed that the addition of CNCs has improved fiber uniformity and decreased fiber diameter. This is attributed to the enhanced electric conductivity of electrospinning solutions in the presence of CNCs. Thermal and mechanical properties of electrospun fiber mats were studied using thermal gravimetric analysis and dynamic mechanical analysis. The addition of CNC produced minimal changes in fibers thermal behavior and resulted in significant improvement to the fibers mechanical properties. PAN-CNC composite nanofibers webs showed an increase in tensile strength compared to neat PAN nanofibers webs.

The pore size distribution of analyzed samples indicated large volume of micropores and mesopores resulting in about 75 % microporosity. Among the tested samples, the maximum surface area and micropore volume are 3,497 m^2/g and 1.04 cc/g for 30% W_{CNC}/W_{PAN}. In addition, the maximum adsorption capacity of the 30% CNC/PAN sample reached 170 % for both adsorbates. Compared to activated carbon fiber cloth and beaded activated carbon, PAN-CNC composite nanofibers depicted faster adsorption kinetics reflecting in higher mass transfer coefficients due to the small fiber diameter. These results showed that CNCs have a distinct advantage for improving the mechanical and adsorption properties of electrospun nanofibers.

I dedicate this dissertation to my beloved parents, my dearest husband, Suheil, and my adorable son, Salem. They have been a constant source of support, motivation, and perseverance for me throughout my life.

ACKNOWLEDGEMENTS

First and foremost, I would like to express my deepest gratitude to my supervisor, Professor Zaher Hashisho, for his supervision, guidance and generous support throughout my course work and research. I highly appreciate his invaluable comments and continuous feedback throughout my MSc research. This work could not have been accomplished without his profound knowledge, guidance and passion.

I would like to also express my deepest gratitude for my co-supervisor, Professor Yaman Boluk, for his guidance and support throughout my research.

I would like to express my deepest gratitude to Professor Rajender Gupta for his permission to use the surface area analyzer.

I would like to acknowledge the financial support from Alberta Innovate Bio Solutions.

I would also like to thank my colleagues in the Air Quality Characterization and Control Lab, for their suggestions and assistance in my experiments.

I am grateful to the technicians in the Department of Civil and Environmental Engineering, Chen Liang and David Zhao, for their help and support during this research work.

Finally, I would like to thank my friends and anyone who directly or indirectly have offered their helping hands in this research.

Table of Contents

List of Tables

List of Figures

List of Acronyms

ACFC	Activated carbon fiber cloth
ACFs	Activated carbon fibers
ACnFs	Activated carbon nanofibers
BAC	Beaded activated carbon
C	Carbon
CAs	Carbon aerogels
CDCs	Carbide-derived carbons
CFs	Carbon fibers
CH_4	Methane
CNC	Cellulose nanocrystals
CnFs	Carbon nanofibers
CNTs	Carbon nanotubes
CO	Carbon monoxide
CO_2	Carbon dioxide
DMA	Dynamic mechanical analysis
DMF	N, N-Dimethyl formamide
DSC	Differential scanning calorimetry
GAC	Granular activated carbon
H	Hydrogen
H_2	Hydrogen

H_2O	Water
HCN	Hydrogen cyanide
IUPAC	International union of pure and applied chemistry
K	Potassium
K_2CO_3	Potassium carbonate
K_2O	Potassium oxide
KOH	Potassium hydroxide
MEK	Methyl ethyl ketone
MV	Micropore volume
N	Nitrogen
N_2	Nitrogen
NH_3	Ammonia
O	Oxygen
PAC	Powdered activated carbon
PAN	Polyacrylonitrile
PEO	Polyethylene oxide
PU	Polyurethane
PVA	Polyvinyl alcohol
PVP	Polyvinylpyrrolidone
SEM	Scanning electron microscopy
SLPM	Standard liter per minute

TGA	Thermal gravimetric analysis
TPCs	Templated porous carbons
VOCs	Volatiles organic compounds
W/V	Weight per volume
W/W	Weight per weight

Chapter 1 Introduction

1.1 Introduction

Adsorption occurs when a vapor, gas, or liquid in contact with a solid material is captured by the solid, either on the outer surface or within the pores of the solid (Bansal & Goyal, 2005). Adsorption is widely used to remove organic compounds from gas streams (Shonnard and Hiew, 2000; Gupta and Verma, 2002; Lapkin et al., 2004) and aqueous systems (Pelekani and Snoeyink, 1999; Dabrowski et al., 2005; Efremenko and Sheintuch, 2006). Adsorption is considered inexpensive, flexible, efficient, and effective even at low concentrations. It has the potential for adsorbent reuse, adsorbate recovery, and multi-pollutant control (Shonnard and Hiew, 2000; Gupta and Verma, 2002; Lapkin et al., 2004).

The most commonly used adsorbents are: activated carbon (AC), zeolite, activated alumina and silica gel. Activated carbon is used for removal of nonpolar gases and organic vapors (e.g., solvents, gasoline vapor, and odors) and H_2 purification. Zeolite is used for drying, H_2 purification, air purification, air separation based on molecular size and shape, and gas chromatography. Silica gel and activated alumina are both commonly used for drying and gas chromatography (Yang, 1987). AC is one of the most frequently synthetized and used adsorbents in air and water treatment due to its cost effectiveness and large surface area (Kawasaki et al., 2004; Alvarez et al., 2005; Aktas and Cecen, 2006). AC is inexpensive and can have high adsorption capacity for organic compounds (Kawasaki et al., 2004; Alvarez et al., 2005; Hashisho et al., 2005; Aktas and Cecen, 2006).

AC is available in many physical forms including fiber, powder, bead, monolith, and granule. This allows using AC in different bed configurations. Activated carbon fibers (ACFs) have shown outstanding performance as adsorbents because of their large surface area and fast kinetic properties (Pré et al., 2002; Chuang et al., 2003; Dwivedi et al., 2004). On the other hand, activated carbon nanofibers (ACnFs) prepared using electrospinning have smaller fiber diameter than ACFs, resulting in larger specific surface area, small pore size, and better kinetic properties than ACFs using the same activation process (Watanabe et al., 2000; Bennett, 2004)

Carbon nanofibers (CnFs) are classified as linear filament with aspect ratio greater than 100. They are attractive one-dimensional carbon nanomaterials because of their low density, high

elastic modulus and high strength (Liu and Kumar, 2012). In addition, CnFs exhibit thermal stability in absence of oxygen, high thermal conductivity, low electrical resistivity (Chung, 2004a, 2012; Rahaman et al., 2011), as well as chemical stability, and biocompatibility (Chung, 2017).

CnFs can be used as electrode materials for lithium (Li) ion batteries, as electrochemical sensors (Baker et al., 2006; Wang and Lin, 2008; Ji et al. 2010), and as scaffolds in regenerative medicine for bones or neural tissues (Ramakrishna et al., 2010). CnFs are fabricated from pitch fibers (e.g., petroleum pitch or coal tar pitch), polymer fibers (e.g., PAN and cellulosic fiber), or carbonaceous gases (e.g., acetylene) (Chung, 2017). Among different techniques to synthesize CnFs, electrospinning is attractive for its versatility and easy process, and has been applied to develop a wide range of polymer and inorganic nanofibers in addition to CnFs. The electrospinning process is carried in air at room temperature to synthesize CnFs, followed by thermal stabilization, carbonization and activation to form activated carbon nanofibers (ACnFs).

Polyacrylonitrile (PAN) is the most commonly used polymer precursor for electrospinning due to its high melting point and large carbon yield (Sanchez-Soto et al., 2001). PAN does not melt when heated but is oxidized into a thermally stable conjugated ladder structure while maintaining its original shape (Niu et al., 2011). Other thermoplastic polymers are rarely used as a carbon precursor due to their severe thermal shrinkage that destroys the fibrous structure (Niu et al.,2011). In addition, electrospun PAN nanofibers are ideal precursors for carbon nanofibers due to their high yield and flexibility. This flexibility allows for the tailoring of the fiber strength and modulus by tuning the carbonization and graphitization temperatures (Donnet et al, 1998). PAN-derived electrospun ACnFs can have unique adsorption properties surpassing many other adsorbents (Sullivan et al, 2012). The adsorption capacity of ACnF was 20 times better than that of granular activated carbon or activated carbon fiber (Sullivan et al, 2012). On the other hand, when comparing carbon fibers (CFs) to CnFs, both made from PAN precursors, CnFs have shown a tensile strength as high as 7 GPa, however CFs have lower mechanical properties (Wang and Kumar, 2006). Because of their significantly enhanced mechanical properties and thermal stability when compared to conventional polymer composites, polymer nanocomposites have been a subject of increasing interest in recent years.

Incorporation of mechanically robust nanoscale fillers such as nanoclays, graphite nanoplatelets, carbon nanotubes and inorganic nanoparticles into polymer matrices has been

extensively explored (Hussain et al., 2006). Utilizing cellulose nanocrystals (CNC) as a reinforcing phase for developing new nanocomposite materials has been recently investigated, and many efforts focused on dispersion of hydrophilic cellulose nanocrystals into hydrophobic polymeric matrices (Eichhorn et al., 2010). CNCs as a reinforcing phase have several advantages over other types of nanofillers, as they are easily modified, inexpensive, renewable, biocompatible, and have remarkable mechanical properties (Dong et al., 2012).

1.2 Objectives

The goal of this study is to prepare CNC-reinforced PAN electrospun activated carbon nanofibers with unique adsorption properties for use in air pollution control.

The objectives of the study are:

1- Optimizing electrospinning conditions to develop defect-free, uniform PAN based nanofiber mats reinforced with CNC
2- Optimizing activation conditions for converting CNC reinforced PAN based electrospun nanofiber mats into ACnFs
3- Characterizing the morphological, thermal, mechanical properties, surface area and pore size distribution of the ACnFs
4- Assessing the adsorption capacity and kinetics of the electrospun activated carbon nanofibers, compared to commercially available activated carbon fiber cloth (ACFC) and beaded activated carbon (BAC).

1.3 Research Significance and Motivation

PAN-originated ACnFs are interesting material because of their high carbon yield, good tensile strength, and presence of nitrogen in the final product, which make them interesting for adsorption applications. Few studies have reported to incorporate nanomaterials like CNCs into the ACnFs matrices to improve their mechanical properties as well as their adsorption effects on

ACnFs. Therefore, CNCs is incorporated into PAN based electrospun nanofiber mats to assess their effect on mechanical strength and their adsorption performance. CNC has been the nanomaterial of choice because of their abundance and unique mechanical, morphological, and chemical properties of CNC make it the most promising biomaterial for industrial applications (Prasanth et al, 2014). In addition, the use of renewable biomaterials for industrial applications is gaining momentum due to the continuously increasing need for alternatives to non-renewable feedstock (Rufford et al., 2013).

1.4 Thesis Outline

This thesis consists of five chapters which will contribute to the overall goal of this research. Chapter 1 provides an introduction, objectives, significance and motivation for this research. Chapter 2 provides a general literature review about cellulose nanocrystals, electrospinning, activation, and adsorption processes. Chapter 3 describes experimental methods and materials. Chapter 4 analyses morphology, thermal behavior, and mechanical properties as well as assess the adsorption properties of ACnFs. Chapter 5 summarizes main conclusions from this research as well as recommendations for future work.

Chapter 2 Literature Review

2.1 Cellulose Nanocrystals

2.1.1 Introduction

For over 150 years, cellulose has been used in the form of fibers or derivatives for a wide spectrum of products and materials. Cellulose constitutes the most abundant renewable and sustainable polymer resource available. It is present in various forms of biomass, such as trees, plants, and tunicate, and can also originate from bacterial sources, the best-known example of which is Acetobacter xylinum (Hamad, 2017).

Chemical hydrolysis or applying large mechanical shear forces onto a cellulose suspension can separate cellulose nanomaterials from the source biomaterial (Olsson et al., 2011). The yield is rod-like crystalline residues known as cellulose nanocrystals. They can be referred as cellulose nanowhiskers or nanocrystalline cellulose. Because of their distinctive properties such as low cost, availability, renewability, lightweight, nanoscale dimension, and distinctive morphology, they have been used as reinforcing agents in nanocomposites materials (Dong et al., 2012). Two general aspects of CNCs are covered in this section, namely their structure and morphology, and their applications in the nanocomposites field.

2.1.2 Structure and morphology

The cellulose molecule is a polysaccharide consisting of β-1, 4-D-linked glucose chains with a molecular formula of $(C_6H_{10}O_5)_n$. The number, n, of the D-glucose unit ranges from 10,000 to 15,000 depending on the source. D-glucose units are bonded through hydrogen bonds that are formed between the oxygen atom of the hydroxyl group of the glucose and the hydroxilic hydrogen atom of the next glucose unit (Samir et al., 2005). The repeated segment is frequently taken to be a dimer of glucose, known as cellobiose that is illustrated in Figure 2.1.

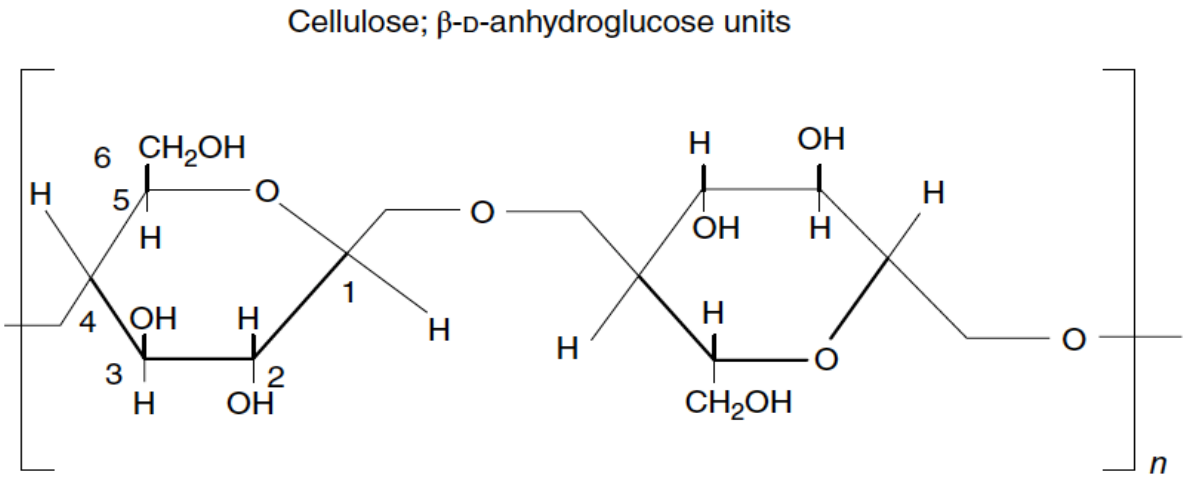

Figure 2.1 Cellobiose, the monomer of Cellulose (Hamad, 2017).

In nature, cellulose molecules exist as microfibrils with a cross-section ranging from 2 to 20 nm, depending on the source (Habibi et al, 2010). Cellulose molecules connect with each other through van der Waals forces and are packed together via intra- and inter-molecular hydrogen bonds. These microfibrils are a mix of disordered or amorphous regions and highly ordered or crystalline regions (Habibi et al, 2010). The amorphous regions of cellulose microfibrils are more susceptible to be attacked by chemical, mechanical and/or enzymatic treatments, in contrast to crystalline domains. Consequently, these microfibrils break down into shorter crystalline components with high crystalline degree and a rod-like structure, that are referred to as CNCs (Habibi et al., 2010). The obtained CNs have similar morphology to the original cellulose fibers. Figure 2.2 shows CNC morhology from different sources.

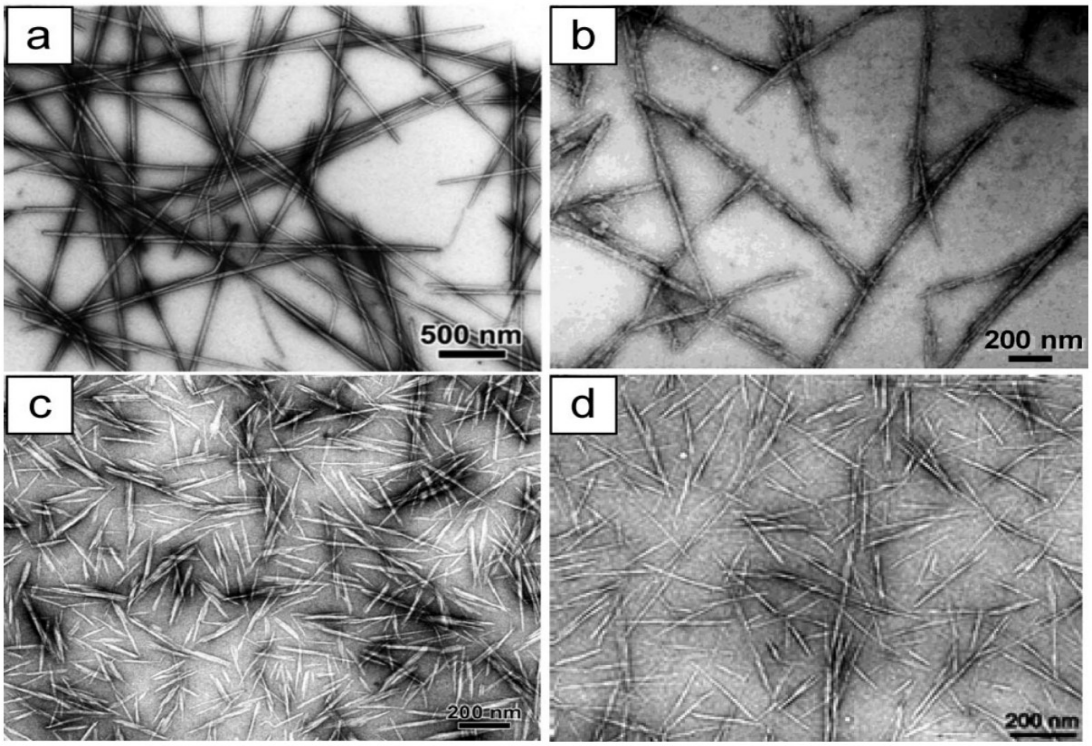

Figure 2.2 TEM image of dried dispersion of cellulose nano crystallites derived from (a) tunicate (b) bacterial (c) ramie (d) sisal (Habibi et al., 2010)

Nowadays, the interest in nanoparticle (<100 nm)-filled polymer composites has grown remarkably since their ability to improve the strength, modulus, elasticity, toughness, and thermal stability of polymer composites (Siqueira et al., 2009). Polymeric nanofibers present an important, and large, class of materials with wide-range of applications in consumer, industrial, and medical sectors. Examples of polymer composite nanofiber includes packaging, paints and coatings, automotive parts, textiles, and structural components—as in windmill, aerospace, and marine applications (Hamad, 2017). Incorporating nanoparticles into polymer matrices is an effective method for reinforcing electrospun nanofibers (Hou et al., 2005; Lu et al., 2009).

CNCs have nanoscale dimensions and excellent mechanical properties. According to Tashiro and Kobayashi (1991), the theoretical value of Young's modulus along the chain axis for perfect native CNCs is estimated to be 167.5 GPa, which is theoretically stronger than even steel and similar to Kevlar. The elastic modulus of native CNCs from cotton and tunicate reach up to 105 and 143 GPa, respectively (Sturcova et al., 2005). In addition, CNCs possess an abundance of hydroxyl groups on their surface, which allow functionalization and facilitate their incorporation

and dispersion into different polymer matrices (Habibi et al., 2010). For these reasons, CNCs are considered one of the ideal nano-reinforcement materials for polymer matrices (Cao et al., 2011; Kvien et al., 2005). These properties make cellulose fibers useful in a wide range of areas, such as filtration, biomedical applications, and protective clothing. In addition, CNCs are considered environmentally friendly material, has high aspect ratio, low density, renewable, biodegradable, and biocompatible (Siro and Plackett, 2010).

CNCs are of interest in composites research for two main reasons: the high strength due to their crystal structure and the high specific surface area due to their nano-scale size. Gao et al. (2015) explain that the mechanical and thermal properties of the nanocomposite fibers are governed by the interfaces between the nanofillers and polymer matrix. The stronger the interactions, the higher is the strength of the fibers. Orts et al. (2005) have shown that the Young's modulus of extruded starch plastics increase by fivefold when 10.3% (w/w) CNC was added. Similarly, electrospun polyethylene oxide (PEO) fibers loaded with only 0.4% bacterial CNC show improved tensile modulus, strength and elongation by 194%, 72% and 233%, respectively (Park et al., 2007). In addition, Wu et al. (2007) demonstrate that a 5% CNC loading in polyurethane (PU) has increased the strength and strain of the solvent cast film from 39 MPa and 157% to 257 MPa and 237%, respectively.

CNCs are charged nanoparticles with high surface area. It is challenging to keep them apart from each other at high concentrations and/or in the presence of nonpolar, hydrophobic polymers (Olsson et al., 2011). CNCs have a high tendency for self-association due to their strongly interacting surface hydroxyl groups. These interactions lead to the aggregation of CNCs which often is undesirable for the preparation of nanocomposites (Olsson et al., 2011). In addition, CNCs have limited solubility in common solvents and inability to melt because of its numerous intermolecular and intra- molecular hydrogen bonding. Essentially, a uniform dispersion of the CNCs and adhesion between the nanofillers and the polymer host matrix generally is fundamental for enhanced mechanical properties of the resulting nanocomposites (Olsson et al., 2011). Therefore, the preparation of CNC-based nanocomposites should be carried out in a solvent, in which the monomers are soluble and dispersible, for instance, the polymerization of acrylamide (Zhou et al, 2011) and acrylic acid (Yang et al, 2012) in water. The following section will address the electrospinning process used to form polymer nanocomposite fibers.

2.2 Electrospinning

Fibers with diameter within the nanometers range, possess several excellent characteristics: very large surface area to volume ratio, surface functionalization, and superior tensile strength when compared to any other form of material. These characteristics make polymer nanofibers an optimal candidate for several applications. A variety of physical-chemical methods can be used to prepare nanofibers. However, specific methods need to be followed when cellulose is added to the polymer solution since cellulose is neither fusible nor soluble in most common solvents (Prasanth et al.,2014). Electrospinning is the best method to synthesize fibrous structures containing nanoscale cellulose. It has several advantages such as cost-effectiveness, and the ability to make nanofiber materials with a diameter ranging between 40 nm to 2,000 nm that possess high surface area to volume ratio. However, electrospinning has a slow production rate, and uses a high voltage which acquires safety concerns (Prasanth et al.,2014).

The origin of electrospinning was discovered by an English physician named W. Gilbert back in 1600. He noticed that in presence of a rubbed amber piece, a water drop changed into a conical shape. He was the first to notice the impact of electric external field on liquid-air interface (Erich et al., 2018). In 1897, the term 'electrospinning' was invented by Raleigh. In late thirties, Petryanov-Sokolov and his collaborators carried out experiments for producing electrospun fibrous materials. This led to the first industry manufacturing filters called Petryanov filters for gas masks (Kim and Reneker, 1999). In a series of patents, Formhals described the experimental setup used to produce polymer fibrous materials using electrostatic forces (Kim and Reneker, 1999). Subsequently, the interest of this process has grown remarkably.

2.2.1 Process

Electrospinning is derived from "electrostatic spinning", in which nanofibers can be prepared from polymer solution using electrostatic force (Prasanth et al., 2014). It is a fiber production method to form fibers with few nanometers diameter and few kilometers of length. A high voltage electric field is applied to the polymeric solution. It charges the polymeric solution to jet into nanofibers. In order for the jet to develop at the needle tip, the charge within the polymeric

solution must reach above the critical voltage. This results in the formation of Taylor's cone (Erich et al.,2018). Critical voltage is when the electrostatic forces overcome the surface tension of the polymer solution. Taylor's cone happens when the surface of the fluid at the needle tip elongates to form a conical shape. It is reached by increasing the intensity of the electrical field. The electrospinning jet travels towards the lower potential grounded collector, where it deposits to form a nonwoven mat. As the jet travels in the air, solvent evaporates, and dry fibers deposit on the collector. For low-viscosity solutions, the jet breaks up into droplets. While for high-viscosity solutions, the jet travels to the collector as fiber jet (Erich et al., 2018).

The electrospinning setup as shown in Figure 2.3, consists of a syringe containing polymer solution with a flat metal tip needle, a syringe pump, a high-voltage power source, and a conductive collector. One electrode of high voltage power supply is placed on the metal tip of the syringe and the other is attached to the collector. Usually, the collector is grounded. The steps involved in the electrospinning process are first synthesis of polymer precursor solution with suitable viscosity and then electrospinning the solution onto a plate and optimizing the parameters such as voltage and distance between the collector and the syringe.

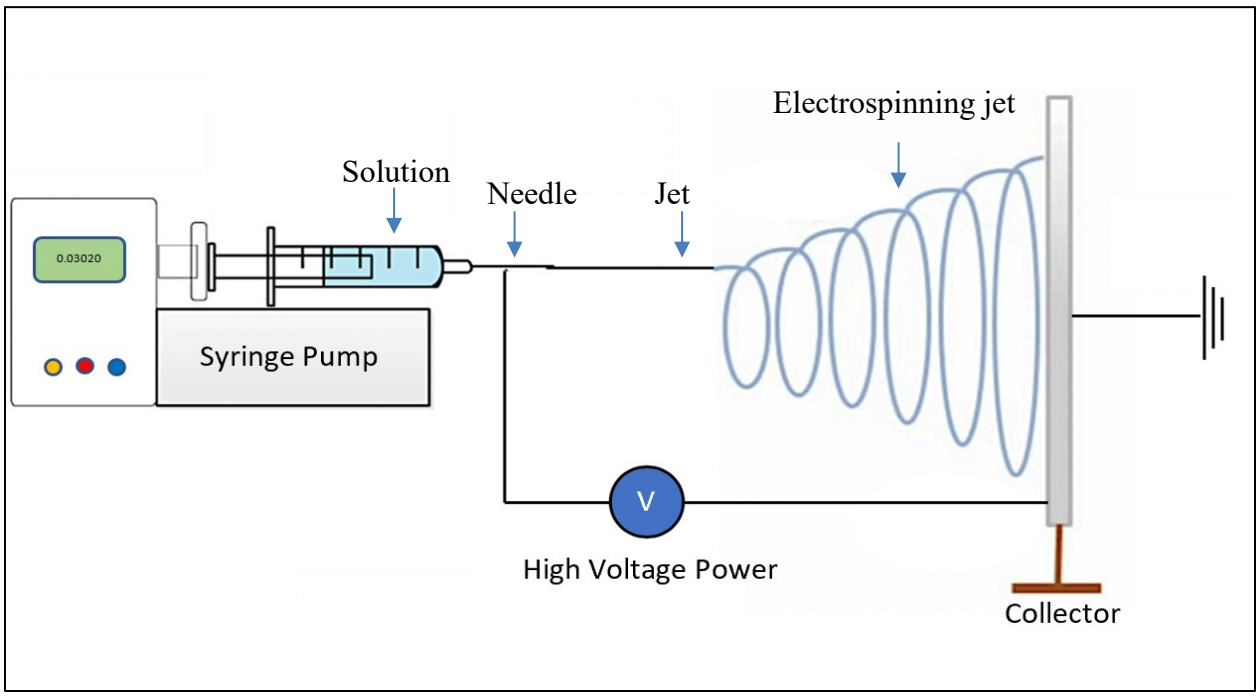

Figure 2.3 Schematic diagram of the electrospinning setup.

2.2.2 Factors controlling electrospinning

Various parameters control the fiber formation. It can be divided into solution related parameters, process related parameters and ambient related parameters as shown in Table 2. (Zahmatkeshan et al., 2018).

Table 2.1 Parameters affecting electrospun polymer nanofibers morphology

Solution related parameters	Molecular weight of polymer Polymer concentration Solution conductivity Solvent volatility
Process related parameters	Applied voltage Distance between tip and collector Flow rate
Ambient related parameters	Temperature Humidity Air velocity

2.2.2.1 Solution related parameters

The most important factors in solution related parameters are viscosity or polymer concentration, polymer molecular weight, solution conductivity, and solvent volatility. Polymer concentration or solution viscosity influences the size, alignment and defects of the fiber. It has to

be optimum for chain entanglement to occur, and it is associated with viscosity and surface tension. The effects of surface tension lead to the formation of droplets at low solution concentration and hence, bead formation occurs instead of fibers. On the other hand, at high solution concentration, droplet is stopped in the needle tip because of viscosity which affects the rate of charged polymer flowing through (Zahmatkeshan et al., 2018).

In addition, some studies (Kai et al., 2014; Ingavle and Leach, 2013; Bhardwaj and Kundu, 2010; Sill and Von Recum, 2008) showed that the higher the polymer concentration the larger fiber diameter and the lower pore size distribution. Altogether, there is an optimum viscosity value for each polymer in electrospinning process, and this characteristic has a significant effect on the fiber morphology and the success of the electrospinning process.

Molecular weight of the polymer is representative of the number of entanglement in the solution and thus its viscosity. In order to produce fibers, high molecular weight polymers are used since they provide the desired viscosity and prevent the effects of surface tension. Low molecular weight solutions tend to form beads instead of fibers. Consequently, solution with low molecular weight polymers electrospray instead of electrospin. On the other hand, high molecular weight polymers result in fibers with a larger average diameter (Ingavle and Leach, 2013).

In addition, solvent characteristics have a great effect on the electrospinning process. The solvent used should have features such as high evaporation rate, low vapor pressure, and low boiling point while preserving polymer solution integrity (Haider et al, 2015). Evaporation rate of the solvent is important since it influences the solvent evaporation while the jet travel from the spinneret to the collection plate. Therefore, volatile solvent should be used. Due to the jet thinning, rapid solvent evaporation and phase separation occur. Thus, solvent vapor pressure plays a critical role in determining the rate of vapor and drying time (Zahmatkeshan et al., 2018).

Finally, polymer solution conductivity depends on the polymer type, solvent used, and the presence of ionizable salts (Ingavle and Leach, 2013). Conductive solutions have a greater charge density compared to low conductivity solutions. Therefore, the fiber jet from high conductivity solutions will be exposed to greater tensile forces and has significant reduction in the nanofiber diameter (Haider et al., 2015).

2.2.2.2 Process related parameters

For process related parameters, applied voltage, flow rate, and distance between tip and collector, are important. Increasing applied voltage results in larger electrostatic forces in the jet, which leads to higher evaporation rate of the solvent, and reduced fiber diameter. Larrondo and Manley (1981) showed that by doubling the applied electric field, the fiber diameter is reduced almost by half. The polymer solution flow rate also affects the diameter and morphology of fibers. High flow rate results in large fiber diameter, while low flow rate results in thinner fiber diameter. At lower flow rate, the solvent has enough time to evaporate. However, at high flow rate there is no sufficient time for solvent to evaporate before reaching the collector plate resulting in electrosprayed particles and beads formation (Bhardwaj and Kundu, 2010; Miao et al., 2010; and Kai et al., 2014;). Therefore, fibers with more uniform diameters can be obtained with a lower flow rate.

Distance between spinneret and collector is also related to morphology and fiber diameter. A minimum distance is required to provide sufficient time for stretching and drying the fibers before reaching the collector. Beads are observed in both close and very far distances. In fact, the distance can determine if electrospining or electrospraying occurred. In addition, nature of the solvent is key in determining the optimal distance. High volatility solvents requires short distance while low volatility solvents require long distance for allowing sufficient evaporation time. In conclusion, a minimum distance, approximately 8– 15 cm, is necessary to form smooth and bead free fibers (Ingavle and Leach, 2013).

2.2.2.3 Ambient related parameters

Ambient parameters such as temperature, humidity, and air velocity also affect the quality of the fibers. Viscosity and temperature are inversely related. By increasing the temperature fiber diameter decreases, which is caused by the reduced solution viscosity. Bae et al. (2013) demonstrated that by increasing humidity, small spherical pores appeared on the surface of the fibers and by further increasing the humidity the pores will be connected. In addition, at very low humidity solvent evaporation rate increases thus the solvent dries very fast. High humidity can lead to the discharge of electrospun solution. The air flow above the needle can also lead to increased evaporation rate through convection which lead to larger fiber diameter (Ashammakhi et al, 2009; Bhardwaj and Kundu, 2010; Ingavle and Leach, 2013).

2.2.3 Polymer used in electrospinning

Large number of natural and synthetic polymers have been successfully electrospun into continuous fibers with a diameter in nanometer scale and a length of several meters (Bhardwaj et Kundu, 2010). The most important characteristics of the precursors for producing carbon fibers are: easy conversion, high carbon yield, and cost-effective processing. Natural polymers commonly used in electrospinning are collagen, gelatin, elastin, silk fibroin, casein, cellulose acetate, chitosan, fibrinogen, and chitin. In medical fields, natural polymers demonstrated better biocompatibility and lower immunogenicity compared to synthetic polymers. On the other hand, synthetic polymers have more advantages then the natural one due to their superior mechanical properties including viscoelasticity and strength (Zahmatkeshan et al., 2018).

The most widely used polymers in electrospinning are polyvinyl alcohol (PVA), polyvinylpyrrolidone (PVP), polyacrylonitrile (PAN), polyamide-6, polyacrylic acid, polyurethane, polyethylene oxide, poly(trimethylene terephthalate), gelatin, collagen, chitosan and silk (Erich et al., 2018). Among the precursors used for the production of carbon fibers, the PAN-based ones are dominant. PAN is a thermoplastic polymer with a glass transition temperature of about 80° C and a melting temperature of about 350° C (Yue & Economy, 2017). Rahaman et al. (2017) demonstrate that PAN-based carbon fibers are stronger than others prepared from other types of precursors (pitch, rayon, etc.) due to their higher melting point and greater carbon yield. In addition, PAN-originated activated carbon fiber (ACF) contains nitrogen in the final product which demonstrate an interesting function as adsorbent and catalyst since nitrogen acts as an active site and can bind with adsorbents (Suzuky et al., 1993).

2.3 Carbonization and Activation processes to produce ACnFs

This section provides an overview of the development of three important processes in manufacturing ACnFs. All ACnFs including the PAN-based carbon fibers are subject to oxidative stabilization, carbonization and activation. Briefly, the conversion of PAN-based carbon fiber follows the following steps.

1- Oxidative stabilization in an oxygen-containing atmosphere at temperature between 180 and 300°C.

2- Carbonization in an inert condition to eliminate the non-carbon atoms.
3- Activation process that can be physical activation (reaction with hot gas, supercritical fluid, or plasma) or chemical activation (using chemical reagents).

2.3.1 Stabilization pretreatment processes

The stabilization step is essential to make the fibers infusible to resist the high temperatures during carbonization. Otherwise, the as-spun fibers would melt, fuse, degrade, or decompose rapidly at high temperatures. The goals in ACFs manufacturing are first keep the fiber form, second increase carbon yield, then improve fiber strength, and finally optimize carbon structure and porosity in the subsequent carbonization and activation processes (Yue & Economy, 2017). During stabilization different chemical reactions such as cyclization, dehydrogenation, aromatization, oxidation, and cross-linking, take place which can result in the formation of the conjugated ladder structure (Bashir, 1991; Dalton et al., 1999).

Usually, PAN fibers are spun using solution spinning rather than melt spinning because degradation of PAN happens prior to its melting point (Yue & Economy, 2017). Therefore, fiber stabilization is crucial is crucial to convert the fibers from a thermoplastic to a thermosetting state to withstand the high temperatures during carbonization (Irvin, 1959). In stabilization, the fibers are heated in an oxygen-containing atmosphere (usually air) at about 200– 350°C for a certain period of time (Yue & Economy, 2017). Paiva et al. (2003) suggested that heat treatment involved in stabilization of PAN fiber is carried out usually in the region of 180- 300°C. When temperature exceeds 180°C, the molecular chains will unfold and move around. On the other hand, some researchers reported that heating temperature within 200-300°C are usually used to stabilize the fiber (Dalton et al., 1999; Ko, 1991; Martin et al., 2001; Sánchez-Soto et al., 2001). Fitzer et al. (1986) suggested that the best stabilizing temperature is 270°C. However, Gupta and Harrison (1997) and Mittal et al. (1997) found that heating treatment needs to be higher than 300°C to complete the stabilization. Ko (1991) stated that PAN fiber with optimum stabilization condition can produce higher modulus carbon fiber than unstablized fiber or than fiber which is prepared at high temperature stabilization process. As a consequence, overheated or fused or burnt fibers can result if the temperature is too high. On the other hand, if the temperature is too low, the reactions

are slow and results in an incomplete stabilization, yielding poor carbon fiber properties. In addition, Mittal et al. (1986) demonstrated that PAN fibers stabilized at low temperature could not withstand high heating rate in later processes and produce brittle fibers. Because stabilisation is an exothermic process, a gradual heating has to be employed. This ensures no sudden release of heat and no excessive weight loss and chain scission, or fusion and burning of the fibres (Rahaman et al., 2007).

During stabilisation, the white fibers turn golden yellow, then orange, then tan-brown, and finally black. The appearance of black color indicates the formation of ladder like structure (Friedlander et al., 1968). HCN as well as CO_2 and water are generated during PAN stabilization reactions; hence, the outlet air must be properly exhausted and treated.

The mechanism behind thermooxidative stabilization of PAN nanofibers is summarized in Figure 2. 2 and includes the following three main steps (Yue & Economy, 2017):

1- Cyclization of the nitrile groups, which involves reaction of nitrile groups to form a ladder structure. The triple bond changes to a double bond. Chemical shrinkage occurs as a result of the cyclization of the CN groups leading to a ladder structure.
2- Dehydration of saturated carbon–carbon bonds, which may precede cyclization, and continue during and even after cyclization. These reactions will lead to weight loss of the PAN fiber, and are responsible for the change in color.
3- Oxidation, which makes the cyclization fast; increases carbon yield; and improves mechanical properties. Several different structures have been proposed, such as carbonyl, oxygen forming bridging ether, carboxylic; hydroxyl group, etc.

In conclusion, upon stabilization, PAN molecules are converted into a cyclized network of hexagonal carbon– nitrogen rings. The incorporation of hydroxyl and carbonyl groups in the structure increases the strength of the bonds, promotes intermolecular cross-linking, and increases the thermal stability of the fiber. These changes prevent the fibers from fusing together (Yue & Economy, 2017).

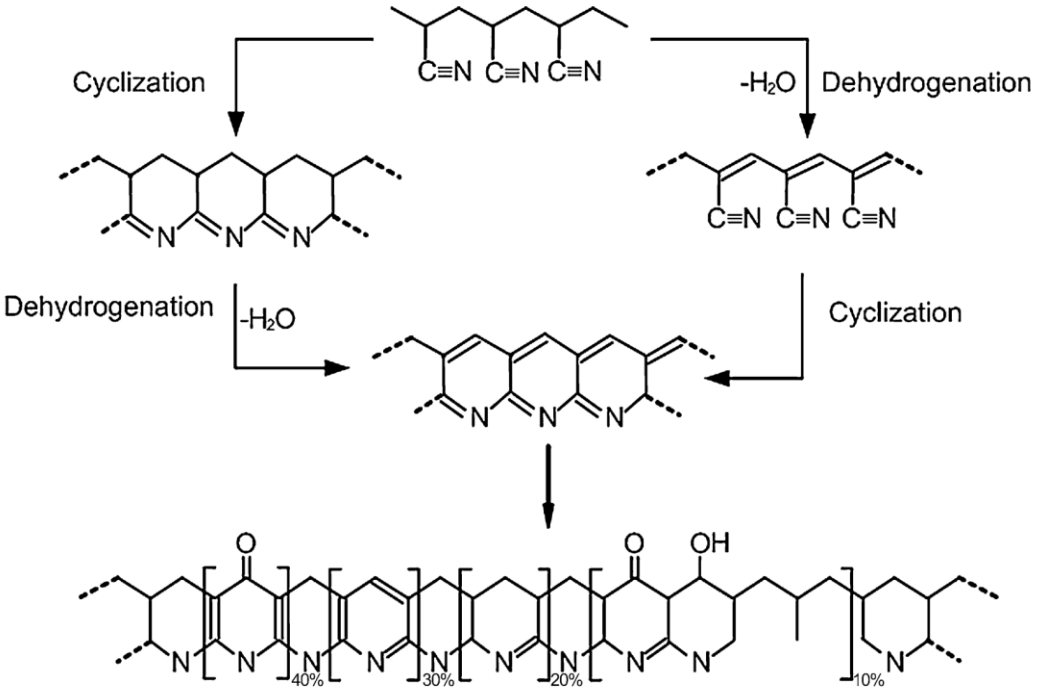

Figure 2.4 Possible reactions that can occur during the stabilization of PAN fiber (Rahaman et al., 2007).

2.3.2 Carbonization process

The carbonization process or pyrolysis is an essential step in manufacturing ACnFs. The stabilized fibers undergo a heating process at a high temperature up to 3000°C, to reach typically to a 95% carbon content and a disordered graphite-like carbon structures (Wu et al., 1987; Ko, 1991). The first step in carbonization process involves thermal pyrolysis for up to 600°C where a low heating rate of 5°C/min is applied. The reason for low heating rate is to slow down the mass transfer and because the stabilized fibers are fragile that they could not withstand high heating rate (Fitzer et al., 1986). In the second stage, high heating rate to reach final temperature could be applied since there is a lower possibility of structure damage (Mittal et al, 1997). However, Chen and Harrison (2002), and Fitzer (1986) claim that too high heating rate could cause higher amount of shrinkage. Hence, optimum carbonization is required in order to form better properties of final carbon fiber.

During carbonization, dehydration, dehydrogenation, rearrangement, condensation, hydrogen transfer, and isomerization take place simultaneously. The precursor materials are

pyrolyzed into a carbon residue which removes the non-carbon atoms from the atomic structure. Volatile compounds such as water vapor, carbon monoxide, carbon dioxide, and hydrogen are released. Yue and Economy (2017) conclude that the pyrolysis temperature controls the degree of carbonization, the carbon content, the microporosity, and the size and degree of disordered carbon structure, which also depends on the nature of the precursors.

Three parameters in the carbonization process determine the quality and the yield of the carbonized fibers. It is the heating rate, the final temperature, and the processing time. The final temperature is usually between 700 and 1100° C. The final carbonization temperature depends on whether the fibers need to be graphitized or activated (Ko et al., 1993; Tsai, 1994). The carbon fibers with graphite structure, which is usually obtained at higher carbonization temperatures, are difficult to activate and to create highly porous ACnFs (Yue & Economy, 2017). In addition, the mechanism of carbonization is strongly dependent on the nature of the polymer precursors. Carbonization of fiber precursors made of PAN polymers is explained in the following section.

Stabilized PAN fibers containing C, H, O, and N are carbonized to remove all noncarbon elements from the fiber. During carbonization, turbostatic (disordered) graphite-like structure within the carbonized fibers is formed due to intermolecular cross-linking occurring through oxygen-containing groups, dehydrogenation, and denitrogenation (Gupta et al., 1991; Rahaman et al., 2007). Volatile byproducts, including H_2O, HCN, H_2, N_2, CO_2, CO, NH_3, CH_4, and other hydrocarbons, are released at elevated temperatures (Fitzer et al., 1986). Consequently, the fiber diameter is reduced with the removal of noncarbon elements (Fitzer et al., 1986; Edie, 1998; Chen & Harrison, 2002; Huang, 2009). Morgan (2005) summarizes the four stages for these as follow:

- Stage I (~–250°C) is associated primarily with H_2O evolution.
- Stage II (300–400°C) is associated with H_2O, NH_3, HCN, and CO_2 evolution
- Stage III (460–600°C) is associated with an increase of NH_3 and H_2O. A rise in the amount of high molecular weight hydrocarbons is also observed.
- Stage IV (600–800°C) is associated with a noticeable rise in H_2 due to cracking of high molecular weight hydrocarbons. This is accompanied usually by a rise in HCN and CO production. At 600–700°C, a decrease in the NH_3, H_2O, and CO_2 evolution is seen due to conversion to C, H_2, N_2, HCN, and CO.

2.3.3 Activation process

The difference between manufacturing ACnFs and CFs is that in ACnFs an activation step is employed instead of the graphitization. The activation process of ACnFs develops accessible porosity in the fibers for adsorption purposes. Morgan (2005) explained that the activation is carried out to open up and enlarge the pores created during the carbonization process and to create some new porosity. Thus, it results in the formation of a well-developed and accessible pore structure with very large internal surface areas. Many different methods of activation have been reported. These can be classified into two broad categories: Physical activation (reaction with hot gas, supercritical fluid, or plasma) and chemical activation (using chemical reagents). In physical activation, reaction with hot gases (e.g. CO_2, steam) is a primary method for making commercial ACnF products. It is a highly efficient and simple process. However, it needs relatively higher temperatures for activation, and the final production yield is relatively low since some carbon atoms are removed during this process (Yue & Economy, 2017). Chemical activation is usually combined with the carbonization process. It is performed at low temperatures wich results in a high production yield and in some cases creates functional groups on the surface (Yue & Economy, 2017).

2.3.3.1 Physical activation

Physical activation is carried out between 500-1200°C. It develops porosity by carbon gasification with oxidizing gas. Removing carbon atoms generates pores, increases the average size of the micropores already accessible to the gas, and opens up closed pores that are formed during carbonization. Factors affecting the degree of porosity are: carbon structure, the original porosity in the carbonized fiber, the presence of catalytic inorganic impurities in the carbon, type of activation gas, activation temperature, activation time, pressure and flow rate of the gas, diameter of the fiber, and gas–fiber contact efficiency (Yue & Economy, 2017).

The most commonly used oxidizing gases are carbon dioxide and water vapor. They can be used either individually, mixed together, or with an inert carrier gas (Yue & Economy, 2017). Other gases, including air and oxygen plasma (Ismail, 1991), NH_3 (Li et al., 2001; Mangun et al., 2001), supercritical water (Salvador et al., 2008), and supercritical CO_2 (Sánchez-Montero et al., 2008; Salvador et al., 2009) have also been used in the preparation of ACFs. Finally, it should be

noted that because the physical activation reaction is determined by the rate of diffusion of the gas, the degree of activation on the fiber surface is usually much higher than that in the core area of the fiber.

2.3.3.2 Chemical activation

Chemical activation is a reaction between the raw material and the activating reagent. The activating reagent could be solid or liquid at room temperature (Yue & Economy, 2017). The fiber could be used as-spun, stabilized, or carbonized. The process consists first of impregnating or mixing the fibers with the activating reagent and then heating at a maximum temperature of 900° C. In chemical activation, carbonization and activation steps proceed simultaneously. After activation, the fibers are washed with deionized water, acidic or basic solutions to remove the residues of activating reagent (Yue & Economy, 2017). Advantages of chemical activation are lower activation temperature and shorter time, higher carbon yield and higher specific surface area (SSA). On the other hand, its disadvantages include the corrosiveness of the chemical reagents and a washing step to remove the chemical agents (Wang et al., 2012). Factors that affect porosity are the nature of the fiber (as spun, stabilized, or carbonized), types of activation reagents, methods of impregnation or mixing, the concentration of activation reagent, temperature and time for simultaneous carbonization and activation.

The most common chemical activation reagents used in the preparation of ACFs are phosphoric acid (Rosas et al., 2009), zinc chloride (Astashkina et al., 2008; Chiu and Ng, 2012), potassium hydroxide (KOH) (Kunowsky et al., 2008; Xue et al., 2011; Díez et al., 2015). Among various chemical reagents, KOH is widely used since it can result in ACs with defined micropore size distribution, high micropore volume (MV), and a very high SSA of up to 3000 m^2/g (Wang and Kaskel, 2012). Moreover, KOH activation is also efficient for generating micropores and small mesopores into various structured carbons, such as CFs, CnFs, carbon nanotubes (CNTs), templated porous carbons (TPCs), carbide-derived carbons (CDCs), carbon aerogels (CAs), and graphene as mentioned by Wang and Kaskel (2012).

KOH activation: Chemical activation is used to increase the SSA, for which KOH is the most powerful and accessible activation agent (Lillo-Ródenas et al., 2003). KOH activation mechanism consists of oxidizing carbon to CO and/or CO_2 and reducing KOH to metallic

potassium (Otowa et al., 1993; Lozano-Castelló et al., 2007). Wang and Kaskel (2012) summarize the chemical reaction in eqn (1-4). At 400°C, K_2O is formed by KOH dehydration (eqn (1)). Then carbon and H_2O react and H_2 is emitted (eqn (2)). K_2O and CO_2 (produced in eqn.3) form K_2CO_3 (eqn (4)).

$$2KOH \rightarrow K_2O + H_2O \quad (1)$$

$$C + H_2O \rightarrow CO + H_2 \quad (2)$$

$$CO + H_2O \rightarrow CO_2 + H_2 \quad (3)$$

$$CO_2 + K_2O \rightarrow K_2CO_3 \quad (4)$$

The overall stoichiometric reaction occurring between carbon and KOH is shown in eqn (5).

$$6KOH + 2C \rightarrow 2K + 3H_2 + 2K_2CO_3 \quad (5)$$

At 700°C or higher, K_2CO_3 formed in eqn (4) and (5), are decomposed into CO_2 and K_2O (eqn (6)), and completely disappears at 800°C. Moreover, the resulting CO_2 can be further reduced by carbon to form CO at high temperature (eqn (7)). K_2O and K_2CO_3 can be reduced by carbon to produce metallic K at temperatures over 700°C (eqn (8) and (9)).

$$K_2CO_3 \rightarrow K_2O + CO_2 \quad (6)$$

$$CO_2 + C \rightarrow 2CO \quad (7)$$

$$K_2CO_3 + 2C \rightarrow 2K + 3CO \quad (8)$$

$$C + K_2O \rightarrow 2K + CO \quad (9)$$

In conclusion, the three main activation mechanisms for KOH activation are (Otowa et al., 1993; Raymundo-Piñero et al., 2005; Lozano-Castelló et al., 2007):

1- The etching of the carbon is responsible for generating the pore network within the activated fibers. This is accomplished by the redox reactions between various potassium compounds as chemical activating reagents with carbon as shown in eqn (5), (8) and (9);
2- The formation of H_2O (eqn (1)) and CO_2 (eqn (3) and (6)) contributes to further developing

porosity through the gasification of carbon;

3- The metallic K (eqn (5), (8) and (9)), intercalates into the carbon lattices of the carbon matrix during the activation. The K intercalation results in expansion of the carbon lattices. After washing off the intercalated metallic K and other K compounds, the expanded carbon lattices cannot return to their previous nonporous structure and thus develop a high microporosity necessary for large SSA and pore volume/ micropore volume.

2.4 Adsorption

Adsorption is when a vapor, gas, or liquid is brought in contact with a solid material and is captured by the solid either on the outer surface or within the pores (Bansal & Goyal, 2005). Adsorption is classified into physical adsorption or physisorption and chemical adsorption or chemisorption. The classification depends upon the nature of the forces involved. In the case of physical adsorption, the adsorbate is bound to the surface by relatively weak van der Walls forces thus the process is reversible. Chemisorption, on the other side, includes exchanging or sharing electrons between the adsorbed molecules and the adsorbent surface, leading to a chemical reaction. The bond between the adsorbent and the adsorbent is a chemical bond and is much stronger than when adsorbed physically. Chemisorption is usually irreversible and upon desorption the original compound may have been chemically changed. Both phenomena can occur simultaneously, while at higher temperatures substances that would normally physically adsorb, may chemisorb to the surface (Treybal, 1980).

Activated carbon materials are made up of a network of pores. The pores are grouped into micropores (diam. < 2 nm), mesopores (diam. between 2 and 50 nm), and macropores (diam. > 50 nm). Usually, adsorption occurs in micropores and only small amount in mesopores and adsorbates pass through the macropores into the mesopores and the micropores surface (Bansal & Goyal, 2005). In adsorption, micropores, mesopores, and macropores play specific role. The micropores determine the adsorption capacity of activated carbon since they represent the largest surface area and pore volume. Micropores are filled at low relative pressure and no capillary condensation take place in micropores. On the other side, the mesopores are filled with capillary condensation at elevated relative pressure. The macropores allow adsorbates to move quickly into

smaller pores located deeper inside the active carbon particles (Bansal & Goyal, 2005). In general, during adsorption, some molecules of the gas become adsorbed while others rebound. At first, the adsorption rate is high since the solid surface is exposed, but as the surface becomes increasingly covered by the adsorbate molecules, the exposed surface available decreases and the adsorption rate also decreases. On the other hand, the rate of desorption of adsorbed molecules increases because desorption takes place from the covered surface. The adsorption rate continues to decrease as desorption rates increase until a balance is reached. At this stage, the solid and the adsorbate are in adsorption equilibrium, and the rate of adsorption is equal to the rate of desorption. It is called dynamic equilibrium as the amount of molecules that stick to the surface is equal to the amount of rebounding molecules from the surface. The equilibrium amount adsorbed is a function of pressure and temperature. If the temperature is kept constant, the equilibrium is called adsorption isotherm which usually used in experimental adsorption (Bansal & Goyal, 2005).

Adsorption on ACnFs: ACnfs are unique and versatile adsorbents. They have excellent properties including remarkable mechanical properties, narrower pore size distribution, higher surface area, smaller fiber diameter which minimizes diffusion limitations and allows rapid adsorption and desorption, excellent adsorption capacity at low concentrations, and excellent flexibility compared to granular activated carbon (GAC) and powdered activated carbon (PAC) (Sullivan et al., 2012; Lee et al., 2013; Wu et al., 2015; Yue and Economy, 2017). Their slit-shaped pores is behind their high adsorption capacity (Lee et al., 2013). Adsorption mainly depends on the surface area, pore structure, as well as surface chemistry that is influenced by both the precursor and the activation process (Ra et al., 2010; Billemont et al., 2013; Qin et al., 2013). Suzuki (1994) reports that ACFs have only micropores therefore adsorbates reach adsorption sites through micropores without diffusion resistance of macropores, which is usually the rate-controlling step in the case of granular adsorbents. In addition, Jaroniec et al. (1991), analyzed nitrogen adsorption isotherms in detail and both cellulose-based and PAN-based ACFs have 85% micropores of uniform size and 15% of fine mesopores.

Particularly PAN-based ACnFs are reported to show some specific adsorption features for acidic materials owing to a trace of nitrogen atoms contained in their structures (Song et al., 2008). In addition, several studies showed that ACnFs derived from PAN have a higher specific surface area, higher loading capacity and high mechanical flexibility. In consequence, they are good

candidates for many applications such as in filters, scaffolds and fuel cells for bio-medical, and energy applications (Arshad et al., 2011; Wang et al., 2012; Inagaki et al.,2014).

Research on adsorption onto ACnFs reinforced with CNC is very limited. Herein, in this study, efforts have been focused on the fabrication, physicochemical properties and adsorption and kinetics of PAN-based ACnFs reinforced with CNC. This new adsorbent material could contribute to the enhancement of more economic and higher adsorption rate of possible contaminants.

Chapter 3 Materials and Methods

3.1 Materials

Cellulose nanocrystal was provided by Alberta Innovates Technology Futures (AITF), Edmonton, AB, Canada. Polyacrilonitrile (PAN) with an average M_w 150,000 g/mol was purchased from Sigma Aldrich and used as a polymer in the electrospinning process. N, N-Dimethyl formamide was purchased from Fischer scientific, with a 99.8% purity, and used as a solvent for PAN/CNC electrospinning solutions. Methyl ethyl ketone and cyclohexane were purchased from Fisher chemicals and used as adsorbate to assess adsorption properties of ACnFs. All reagents were of analytical grade and used as received.

3.2 Reference adsorbents

Reference adsorbents selected for comparison to ACnF are activated carbon fiber cloth (ACFC) (ACC-5092-15; American Technical Trading, Inc.) and beaded activated carbon (BAC; G-70R; Kureha Corporation). The ACC-5092-15 represents a "medium" level of activation.

3.3 Preparation

3.3.1 Solution preparation

N, N-dimethyl formamide (DMF) is considered as the most suitable electrospinning solvent among various organic solvents due to a proper boiling point (153°C) that allow solvent evaporation during electrospinning and excellent conductivity (conductivity = 10.90 µS/cm, dipole moment = 3.82 Debye) (Chen & Harrison, 2002; Fukushima et al., 2006). Therefore, DMF is the solvent used in this study. PAN was the polymer of choice since several studies reported PAN based fibers have high strength, high carbon yield, and slow rate of weight loss during carbonization (Bahl & Manocha, 1974; Donnet & Bansal, 1984; Wangxi et al., 2003). PAN powder was added to DMF solvent to make a solution. PAN concentration in solution was 1, 5, and 10 % W/V with respect to DMF volume. The mixture was stirred at 50 °C then dried CNC was added to PAN solution and the mixture was vigorously stirred for 24 hours at 50 °C to make a suspension. The CNC loading percentage was 0 to 50% (w/w, CNC/PAN) with a 10% increment. After 24 hrs at 50 °C, the solutions were allowed to cool before electrospinning. The detailed composition of the prepared solutions is shown in Table 3.1

Table 3.1 Composition of electrospinning suspensions

Sample	*C_{PAN} (wt.%)	*C_{CNC} (wt.%)
1%PAN	1	0
5%PAN	5	0
10%PAN	10	0
10%PAN-10%CNC	10	10
10%PAN-20%CNC	10	20
10%PAN-30%CNC	10	30
10%PAN-40%CNC	10	40
10%PAN-50%CNC	10	50

*C_{PAN} is the concentration in the PAN/DMF suspension. C_{CNC} is the content based on PAN weight.

3.3.2 Electrospinning process

Pure PAN solutions or PAN/CNC suspensions were loaded in a 10 mL BD plastic syringe Luer Lock with a 20 gauge (inner diameter [ID] = 0.603 mm) stainless steel blunt needle tip. The needle was connected to a high voltage power supply (ES30P=5W, Gamma High Voltage Research, FL), which generates positive DC voltages up to 30 kV. The positive DC voltage was fixed at 18 kV. The flow rate of the solution was controlled by a syringe pump (78-8101, Kd Scientific, USA) and was set to 10 μL/min . An aluminum foil-covered metal plate, acting as an electrode, was placed vertically to collect the nanofiber at a needle tip-to-plate distance of 15 cm (Liu and Adanur, 2010). Optimum voltage, injection rate, and the distance between the spinneret and the collector, as found by Kalantari (2018) were used. Under the accelerating voltage, polymer jets were stretched by the electrostatic forces; solvent evaporates, and nanofibers were formed and deposited on the aluminum foil; as a results, electrospun PAN and PAN/CNC nanomats were formed. The nanomats

are designated as 1%PAN, 5%PAN, 10%PAN, 10%PAN-10%CNC, 10%PAN-20%CNC, 10%PAN-30%CNC, 10%PAN-40%CNC, 10%PAN-50%CNC. The setup used in this study is illustrated in Figure 2.3 presented in Chapter 2.

3.3.3 Stabilization, carbonization and activation

The electrospun nanofibers were peeled off from the collector and were stabilized, activated and carbonized in order to produce ACnFs. Figure 3.2 shows the morphology of the CnFs, as prepared, after stabilization, and after activation.

Electrospun CnFs **Stabilized CnFs** **Activated and carbonized ACnFs**

Figure 3.1 Form and shape of electrospun CnFs, stabilized, and activated and carbonized ACnFs

Stabilization: The electrospun nanofibers were peeled off from the collector and were stabilized in a tube furnace (Figure 3.2). Stabilization was carried out by heating from room temperature to 280°C at a rate of 1°C/min and holding for 4 hrs under 0.2 SLPM in air flow (Liu and Adanur, 2010). This step is essential to make the fibers infusible to withstand the high temperatures during carbonization.

Activation agent: Chemical activation was carried by soaking and mixing of stabilized PAN and PAN-CNC composite nanofibers in KOH solution for 2 hours, followed by drying at

85 °C until water was completely evaporated. The weight ratio of KOH to stabilized PAN and PAN-CNC composite nanofibers was 1. Lee et al. (2004) reported a 2,545 m^2/g SSA for the KOH/stabilized PAN-based fiber ratio of 1:1 and activated at 800°C. A sudden reduction of SSA was observed when KOH/stabilized PAN-based fiber ratio was 2:1 and 3:1. It is believed that excess in KOH destroy micropores walls instead of forming mesopores (Lee et al., 2004).

In a typical preparation scenario, 1g of KOH was dissolved in 100 mL of distilled water and then 1 g of stabilized PAN-based nanofibers was added to the mixture allowing soaking and mixing of the stabilized fibers for 2 hours before putting them into an oven to dry the excess of water.

Activation and carbonization: The stabilized electrospun PAN and PAN-CNC composite nanofibers containing KOH were activated at 800°C at a heating rate of 5°C/min and holding for 2 hrs under 0.2 SLPM N_2 flow to generate micropores within the fibers. The residual KOH on fibers was neutralized with hydrochloric acid (HCl) and the extra HCl was rinsed with distilled water (Liu and Adanur, 2010).

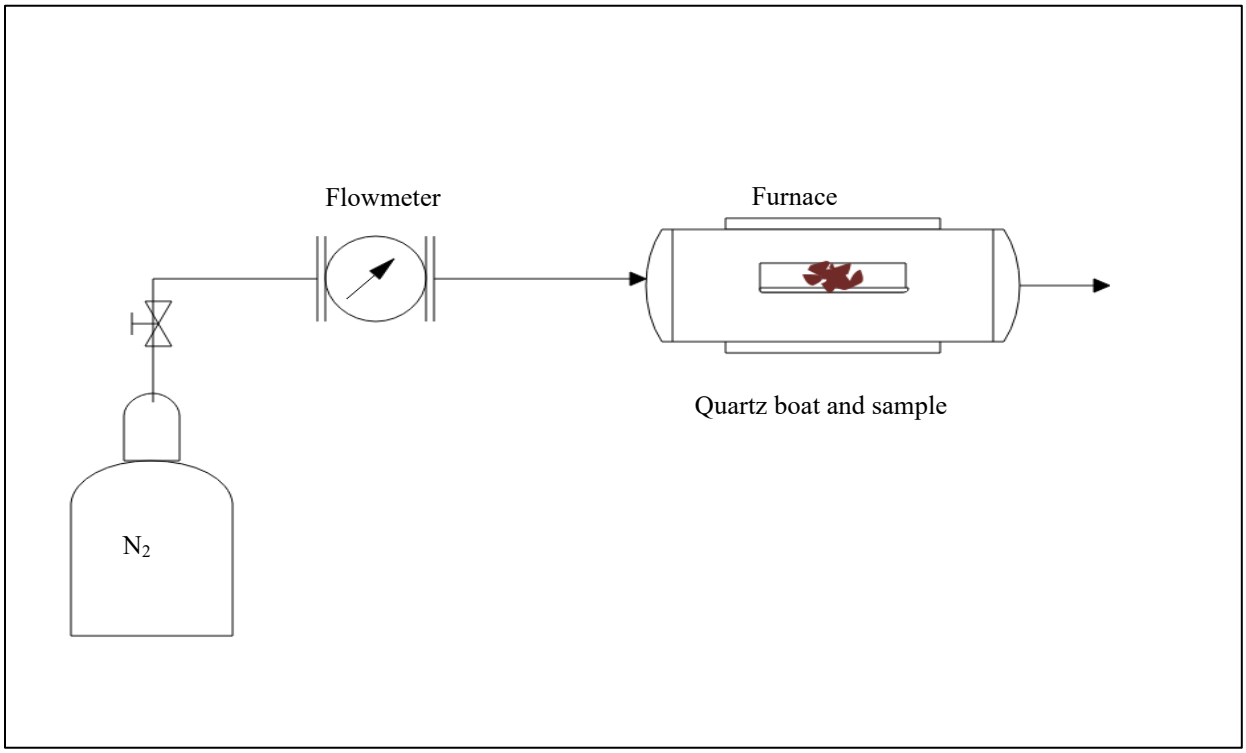

Figure 3.2 Schematic diagram of the activation setup

3.4 Characterization

To determine the success of fiber formation, characterization of the structure and properties of the activated nanofibers was completed using Scanning Electron Micrographs (SEM), Thermogravimetric Analysis (TGA), bulk elemental analysis, X-ray photoelectron spectroscopy (XPS), dynamic mechanical analysis, N_2 adsorption isotherm as well as gravimetric adsorption isotherm and kinetics measurements.

3.4.1 Scanning electron microscopy

Morphology of the electrospun nanofibers was observed by Field Emission scanning electron microscope (SEM) (VEGA3 RESCAN), with an accelerating voltage of 20 kV and a working distance of 20 mm. Samples were prepared by loading the electrospun nanomats onto carbon tape located on an aluminum disk. The samples were gold sputtered and then loaded into the sample chamber where they were analyzed. Using ImageJ analysis software, 20 measurements were taken from the samples to determine the average fiber diameter.

3.4.2 Thermogravimetric analysis

The thermal stability of powder PAN, powder CNC, and electrospun fibers were assessed using derivative thermogravimetric (DTG) analysis (TGA/DSC 1, Mettler Toledo) to optimize stabilization conditions. Approximately 8 to 10 mg of the samples were loaded in the open platinum pan and heated from room temperature to 800°C at a heating rate of 2°C/min and then an isothermal heating at 800°C for two hours. Nitrogen at 50 ml/min was used to purge the samples. DTG was used to determine the weight loss pattern of the samples as a function of temperature.

3.4.3 Bulk elemental analysis

Elemental composition of electrospun nanofibers before and after carbonization was measured with Organic Elemental Analysis (OEA) (Flash 2000, Thermo Fisher Scientific Inc.), using furnace and gas chromatograph column temperatures of 950 and 65 °C, respectively. He as carrier

gas flow was 140 ml/min, He as reference gas flow was 250 ml/min, and O_2 flow rate was 100 ml/min. A 5 sec oxygen dose was used and the run time was 12 min.

3.4.4 Surface elemental composition

Surface elemental composition (C, O, and N) of ACnFs was determined with X- ray photoelectron spectroscopy (XPS) using an AXIS 165 spectrometer (Kratos Analytical). High resolution scans with signal to noise ratio of greater than 10 were obtained for binding energy ranging from 1100 eV to 0 with analyzer pass energy of 20 eV and a step of 0.1 eV. CasaXPS software was used to process the XPS scans and the results are reported in atomic concentrations.

3.4.5 Dynamic mechanical analysis (DMA)

Tensile strength and elongation at break were measured using the TA AR2000 rheometer (TA Instruments, New Castle, DE, USA). Mats were carefully cut into rectangular pieces. The ends of each mat were fixed onto the top and the bottom area of the clamp. After mounting, clamp screws were firmly tightened. The tensile gauge length was 10 mm. The speed of tensile testing was 100 μm/s and three specimens with a length of 15 mm, width of 5 mm, and thickness of 0.2 mm were used for each sample group. The stress and strain were calculated using the machine-recorded force and displacement based on the initial cross-sectional area and gauge length, respectively.

3.4.6 Surface area and pore size distribution

Micropore surface analysis (Autosorb, Quantachrome) was used to characterize the porosity of prepared materials. 20 – 30 mg of samples placed in a 6mm cell were degassed at 150°C for 5 h to remove adsorbed moisture before analysis. After degassing, adsorption of N_2 was performed at -196°C with relative pressure (p/p_0) ranging from 10^{-7} to 0.99. Specific surface area was obtained using the BET equation from relative pressures ranging from 0.01 to 0.07. Micropore volume and pore size distribution were determined using the v-t model, and the pore size distribution using the quenched solid functional theory (QSDFT). The average micropore width was determined for pore widths $\leq$ 20 Å, and the total pore volume was determined at P/P_0 =0.99 using the bulk liquid density for N_2 (0.808 cm^3/g).

3.4.7 Gravimetric adsorption isotherm

MEK and cyclohexane were used as adsorbate to assess the adsorption properties of the ACnFs compared to ACFC-15 and BAC. The adsorption isotherms were obtained gravimetrically using a microbalance (CAHN C-1000) at 22°C with N_2 carrier gas and varying concentrations of MEK and cyclohexane (Figure 3.2). The system logged the equilibrium weight of the sample (40-60 mg) in response to a step change in MEK and cyclohexane concentration (0.01 – 0.8 relative pressure). Equilibrium for a given MEK or cyclohexane concentration was assumed when the weight change was < 0.001 wt.% in 5 min.

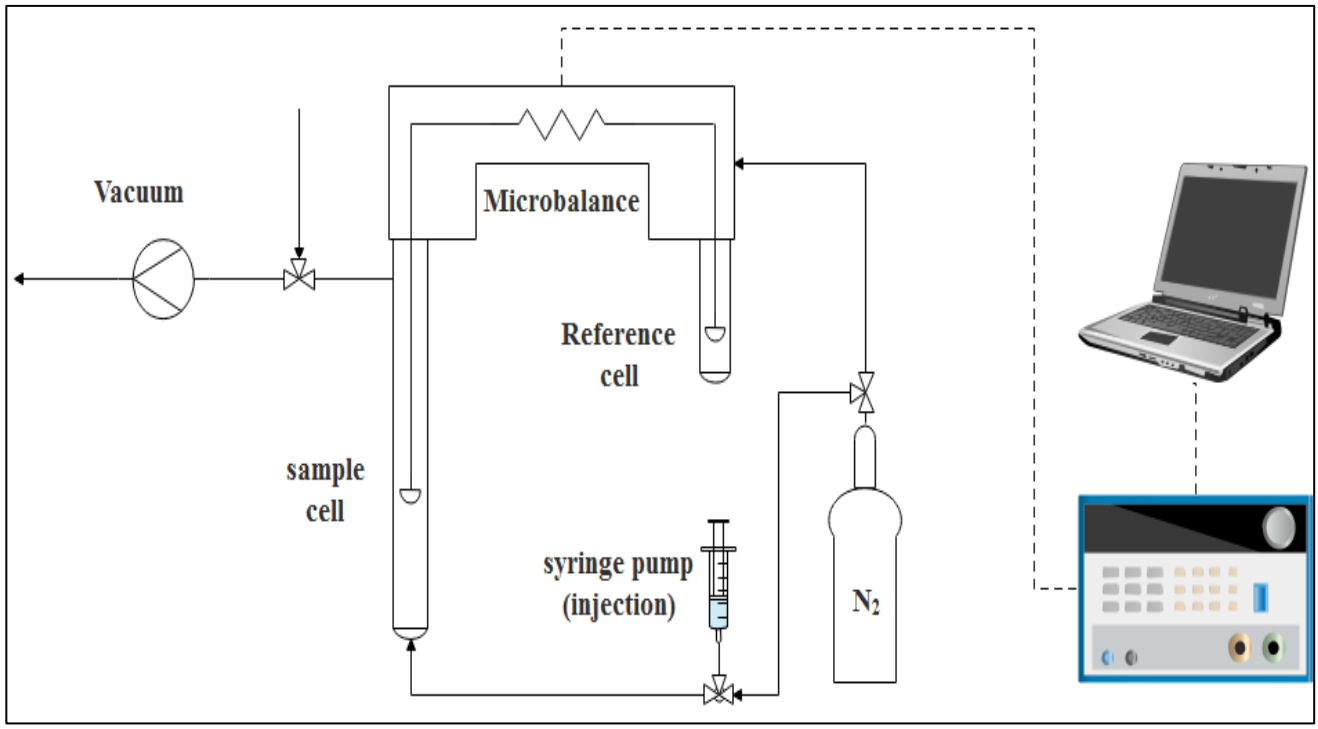

Figure 3.3 Schematic diagram of the adsorption isotherm measurement setup

Each sample was dried in an oven at 150°C and then mounted inside a vertical quartz tube (7.3 cm inner diameter, 40 cm length) to prevent exposure to ambient air. Prior to measuring the adsorption capacity, the sample was flushed with N_2 grade 5.0 until static weight was achieved (<0.03 % change in 10 minutes). A syringe pump was used to inject liquid organic compound into a dry N_2 stream maintained at 300 Standard Cubic Centimeter per Minute (SCCM) (standard

conditions are 25°C and 1 atm). Liquid injection rates were determined using the ideal gas law to generate the desired concentrations. Adsorption was started by introducing the gas stream containing the organic vapor into the adsorption cell containing a 50 mg of ACnFs fiber mats. The form of the ACnFs is shown in Figure 3.1. The data logger recorded the sample weight during adsorption at 1 min intervals, and the adsorption capacity was calculated as follows:

$$Adsorption\ Capacity = \frac{adsorbent\ weight\ after\ adsorption - adsorbent\ weight\ before\ adsorption}{initial\ weight\ of\ adsorbent} * 100\%$$

3.4.8 Adsorption kinetics

Gravimetric equilibrium isotherm data were used to calculate the adsorption rate constant in order to evaluate kinetics of adsorption. After each step change in concentration, the adsorbent weight exponentially approached a new equilibrium. Accordingly, kinetics of adsorption can be determined by using the change in sample weight as a function of time under constant adsorbate concentration and temperature using an appropriate kinetic model or equation. In the present work, the Avrami's equation is used (Calvete et al., 2009):

$$W_t = W_0 + dW(1 - e^{-kt})$$

Where, W_t is the weight of the sample at time t, W_o is the sample weight at t=0, dW is the uptake at equilibrium or adsorption capacity, t is time and k is the adsorption rate constant. Using excel solver values of W_o, dW and k that best fit the weight-time data for a given constant concentration step can be found. Pseudo-first-order kinetic model is assumed (Azizian, 2004). The time to reach equilibrium depends on the adsorbate–adsorbent system, temperature, and step change in concentration. The adsorption kinetics measurements for each sample were collected with the same adsorbate and similar concentrations, temperature, and concentration step change to ensure consistency. The intent is to provide a comparative screening of the kinetics of this new nano-structured material that might serve as a driver for further studies.

Chapter 4 Results and Discussion

4.1 Morphological characterization of PAN nanofiber mats reinforced with CNC

4.1.1 Effect of polymer concentration

A series of samples containing different PAN concentrations were electrospun, resulting in various fiber morphologies, as shown in Figure 4.1. The morphology of beads changed from spherical to more spindle-like as the PAN concentration increased. By further increasing the $W_{t.}$% of PAN from 1% to 10% PAN in 100 mL DMF, the bulge of spindle-like beads disappeared, resulting in more uniform fibers. These observations are consistent with previous results reported by Jeun et al. (2005) and Aslanzadeh et al. (2016). In addition, elongation of beads as well as the fiber diameter increased as PAN concentration increased. This reflects that, at low viscosity, beads are formed along the fiber; and at higher viscosity, the solution is fully stretched by the electrospinning jet leading to beads free fibers. Viscosity is related to the chain entanglements among polymer chains in solution. The degree of chain entanglement is necessary to stabilize the jet. As the concentration of polymers in solution increases, its viscosity increases, which results in more chain entanglements as well as larger fiber diameter (Deitzel et al., 2001; Demir et al., 2002; Ramakrishna et al., 2005). As a result, further solution preparation in this study was carried out using the 10% loading weight for PAN.

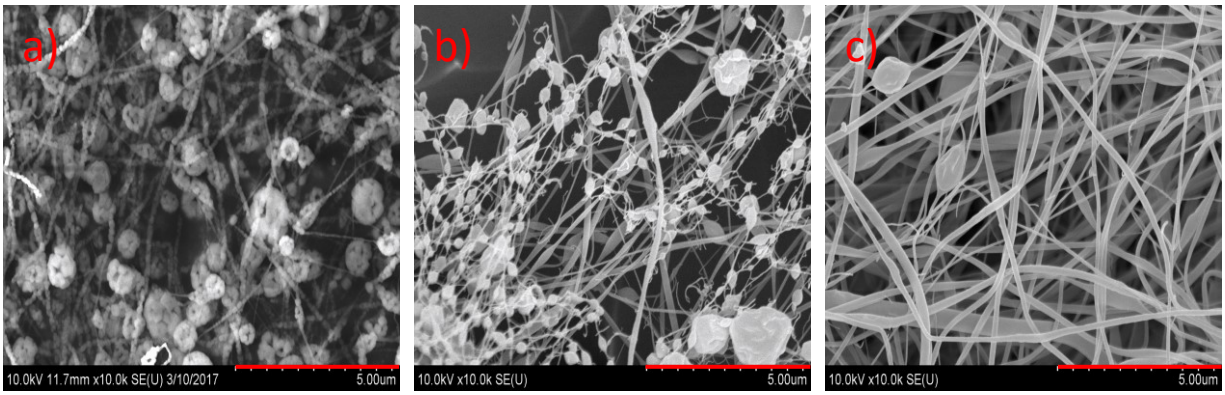

Figure 4.1 SEM micrographs of electrospun PAN nanofibers prepared with different PAN concentrations. PAN concentration: (a) 1%; (b) 5%; (c) 10%.

4.1.2 Effect of % CNC loading

A critical concentration of polymer solution must be exceeded in electrospinning because large chain entanglements are necessary to produce electrospun fibers. On the other hand, if the solution concentration or solution viscosity is too high, electrospinning becomes hard as it is difficult to form a liquid jet (Jeun et al., 2005). In this study, therefore, 10%PAN-40%CNC, 10%PAN-50%CNC did not form fibers but formed large droplets that got attached to the collection plate.

Figure 4.2 shows SEM micrographs at 30,000 magnifications of the electrospun 10%PAN, 10%PAN-10%CNC, 10%PAN-20%CNC, and 10%PAN-30%CNC nanofibers. These nanofibers showed a mat of randomly arranged long, linear nanofibers. The random arrangement of the fibers resulted in low aerial density. The nanofibers had a smooth surface morphology and uniform diameter along their length with some beads or spheres appearance. The formation of beads or spheres may have been driven by surface tension, when the electrical jet underwent a capillary breakdown into droplets. Similar results were reported by Zussman et al. (2015) when electrospinning PAN in DMF solution.

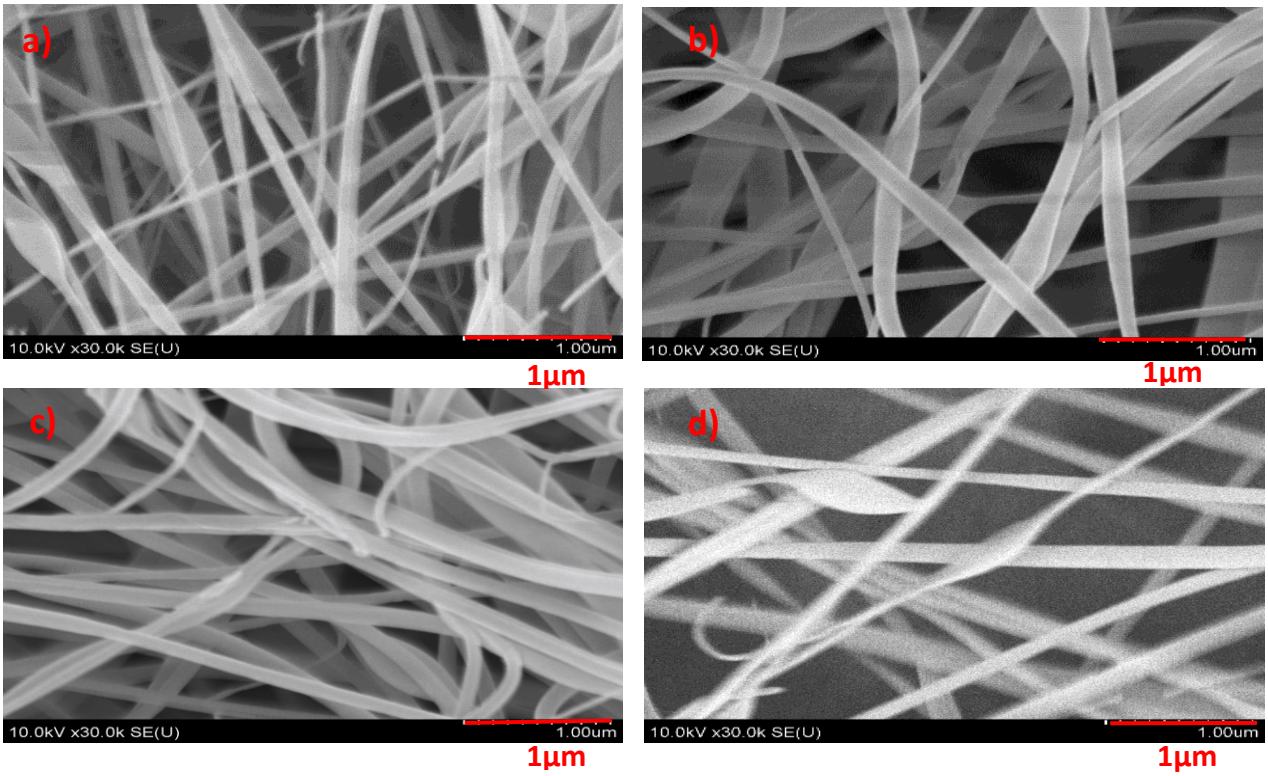

Figure 4.2 SEM micrograph of electrospun PAN-CNC composite nanofibers at 30,000 magnification: a)10%PAN, b) 10%PAN-10%CNC, c) 10%PAN-20%CNC, d) 10%PAN-30%CNC.

Table 4. 1 reports the average size diameter of the electrospun PAN nanofibers using 20 measurements for each sample. The range of average diameter is between 98 to 121 nm. With increasing CNC content in the nanofibers, the average diameter decreased. Peresin et al. (2010) state that to the addition of CNCs increase solution conductivity as a result of the negative charges from the sulfate ester groups on their surfaces. These sulfate groups were originated on the surface of CNCs during production via acid hydrolysis. Haider et al. (2015) explain that with increasing solution conductivity, more filament stretching happens during jet formation leading to decrease in fiber diameters. Similarly, nanofibers diameter decreased when CNC was added to the electrospinning solution of poly (vinyl) alcohol polymer (PVA) (Peresin et al., 2010).

Table 4.1 Average diameters and standard deviation of electrospun PAN-CNC composite nanofibers. Values are reported as average of 20 runs ± standard deviation

Sample	Diameter (nm)
10%PAN	98 ± 38.3
10%PAN-10%CNC	121 ± 40.5
10%PAN-20%CNC	114 ± 30.7
10%PAN-30%CNC	105 ± 44.2

4.2 Thermal properties of PAN-CNC composite nanofibers

Thermal properties of powdered CNC, PAN nanofibers and PAN-CNC composite nanofibers were analyzed by TGA in order to investigate the effect of CNC on the thermal stability of the composite nanofibers. As Tang et al. (1964) note, the predominant mechanism for the conversion of cellulose to carbon includes 4 stages. Stage I. Physical desorption of water (40-150°C). Stage II. Dehydration from the cellulose unit (150-240°C). This involves removal of the hydroxyl and hydrogen groups in the equatorial position of the cellulose molecule, resulting in an intramolecular dehydration and formation of C=O and C=C bonds. Stage III. Thermal cleavage of the glycosidic linkage and scission of other C-O bonds and some C-C bonds via a free radical reaction (240-400°C). This leads to the formation of large amounts of tar, H_2O, CO, and CO_2. Stage IV. Aromatization (400°C and above) where there is negligible to no weight loss.

Figure 4.3 shows the TGA curve of powdered CNC. The % weight loss was about 83%. The weight loss could reach over 90% if the heating rate is higher than 5°C/min as demonstrated by Nuraje et al (2013).The DTG curve of the CNC sample is reported in Figure 4. 4. Initially, the curve showed a low intensity peak at around 50°C corresponding to the loss of water absorbed, a

sharp peak at 280°C marking the cleavage of glycosidic linkage, and a broad peak of low intensity centered at 330°C marking the aromatization process.

In the case of PAN nanofibers, thermal decomposition generally induces chemical reactions, such as cyclization, degradation and thermal cross-linking. In addition, the degradation process of PAN nanofibers is exothermic and is accompanied by the evolution of the volatile gaseous products (Ouyang et al., 2008). As Ouyang et al. (2008) note, the TGA curve of PAN nanofibers is divided into three steps. Step I. Cyclization (up to about 250°C), where weight loss is very small. During cyclisation, the triple bonds of nitrile groups change into double bonds leading to a ladder-like structure. Step II. Dehydrogenation (up to about 300°C), where weight loss is rapid. During this step, chemical reactions occurs and volatile gases are released. Step III. Polymer chains fragmentation (above 400°C), where polymer chains fragmentation produces volatile particles and leads to weight loss.

Accordingly, the TGA curves of 10%PAN nanofiber in Figure 4.3 showed that cyclization of the pendant nitrile group occurred at 260°C leading to a ladder-like structure. This proceeded with small weight loss (as in Ouyang et al., 2008 and Yue and Economy, 2017). Dehydrogenation occurred up to 330 °C, and the weight loss was about 50%. Polymer chains fragmentation occurred above 412 °C, and a steady decrease in weight was observed. The total % weight loss of the 10%PAN nanofiber sample was about 68%, indicating complete evaporation of polymer chain fragments from the PAN nanofibers since no more weight loss was observed. The DTG curve of the 10%PAN nanofiber in Figure 4.4 showed likewise a sharp peak at 260°C and a broad peak of low intensity centered at 412°C. Nuraje et al. (2013) reported that an exothermic reaction ranging between 200 and 450°C, in an inert atmosphere, is typical of PAN.

The effect of CNC concentration on the thermal stability of nanofibers is shown in figure 4.3. When the CNC concentration is 10 and 20 wt%, the PAN-CNC composite nanofibers showed similar weight loss compared to 10%PAN nanofibers. However, the 30 wt% CNC loaded composite nanofibers showed about 17% higher weight loss compared to PAN nanofibers. Similar results were presented by Chang et al (2019). Luo et al. (2018) explained that incorporation of CNC in the nanofibers mats, help provide a pathway for oxygen in the PAN nanofibers mats. This would lead to more homogeneous stabilization and more thermal stability.

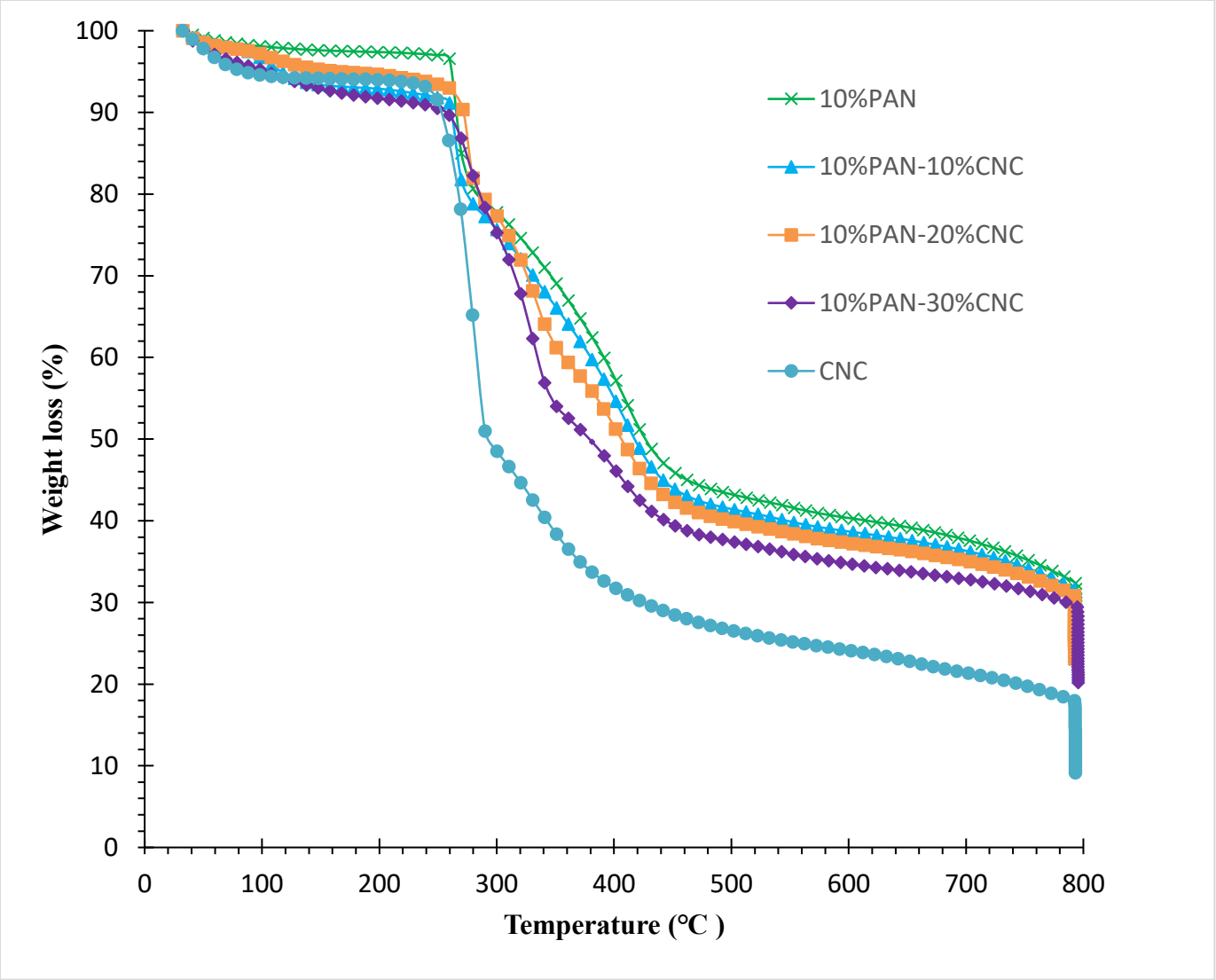

Figure 4.3 TGA curves of powdered CNC and PAN-CNC composite nanofibers

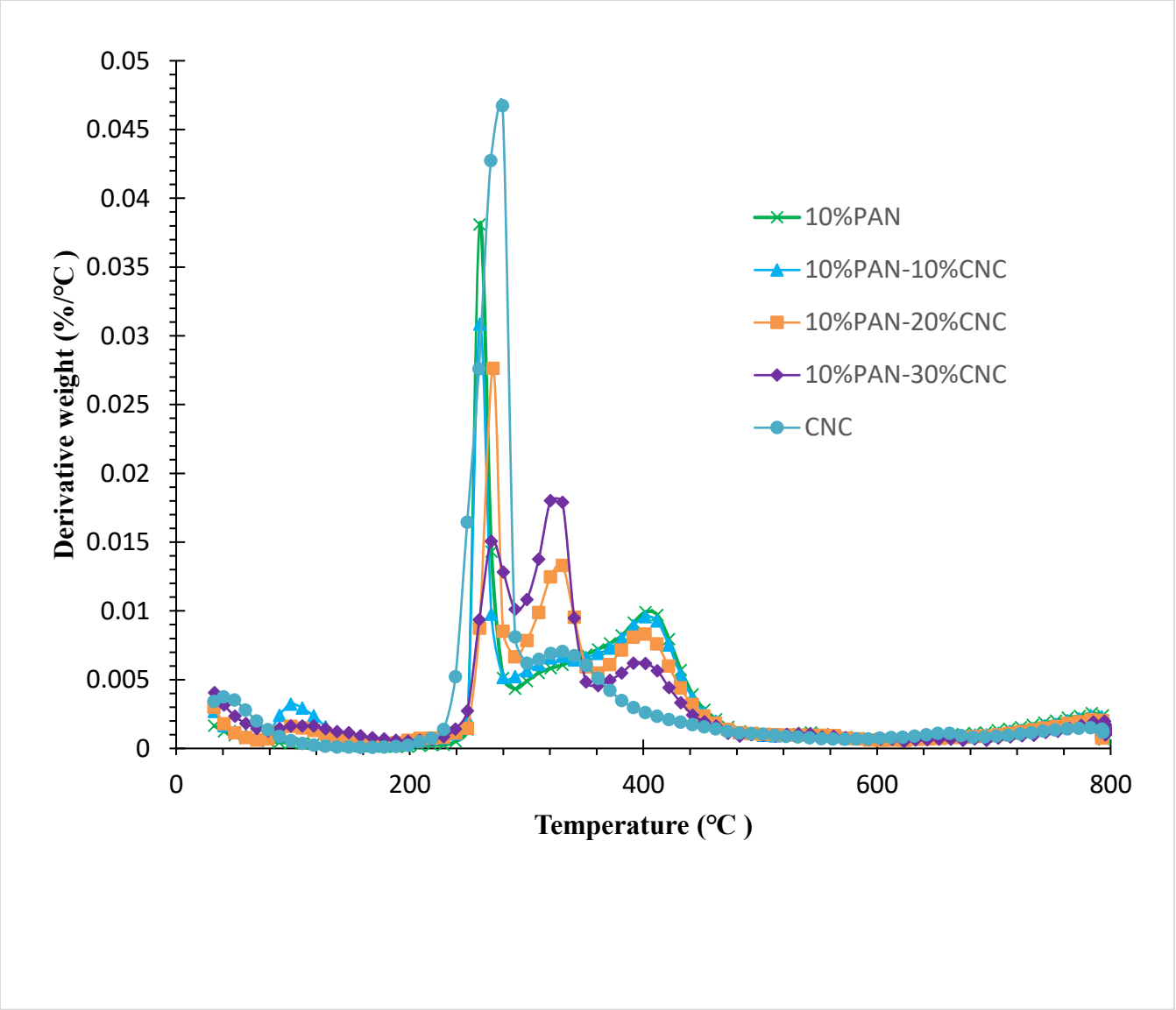

Figure 4.4 DTG curves of powdered CNC and PAN-CNC composite nanofibers

Thermal parameters, including onset thermal degradation temperature, the maximum thermal degradation temperature (T_{max}), and % residue for samples containing different CNC loading are summarized in Table 4.2. The onset thermal degradation temperature is defined as the temperature corresponding to 10% weight loss ($T_{10\%}$). $T_{10\%}$ was 270°C for 10%PAN nanofibers and 249°C for powdered CNC. The addition of CNCs increased $T_{10\%}$ to 280°C and 271°C for 10%PAN-10%CNC and 10%PAN-20%CNC, respectively. However, for the 10%PAN-30%CNC, $T_{10\%}$ value has decreased to 260°C, indicating that its heat resistance decreased. T_{max} for the different nanofibers' mats remained unchanged since the maximum temperature of CNC

decomposition is at 330°C which is well below 400°C, the temperature at which polymer chain fragmentation of PAN occurs. The % residue represents what remains after the mass loss during thermal treatment. CNC depicted the lowest % residue. Addition of CNC into PAN nanofibers, has decreased the % residue with the increase of CNC in the sample.

In summary, the structural and chemical breakdown of the CNC has shifted to higher temperatures for the PAN-CNC composite nanofibers as compared to CNC. However, incorporating CNC into PAN nanofibers resulted in little effect on nanofibers thermal stability.

Table 4.2 Summary of TGA and DTG of powdered CNC and PAN-CNC composite nanofibers. Values are reported as average of two runs ± standard deviation

Sample	$T_{10\%}$ (°C)	T_{max} (°C)	Residue (%)
CNC	249.3 ± 0.5	330.8 ± 0.3	9.14 ± 2.0
10%PAN	269.9 ± 0.4	401.7 ± 0.5	24.4 ± 1.8
10%PAN-10%CNC	279.9 ± 0.9	401.5 ± 1.2	23.1 ± 1.9
10%PAN-20%CNC	271.3 ± 1.4	401.4 ± 0.8	23.1± 2.2
10%PAN-30%CNC	259.6 ± 2.1	401.7 ± 1.7	20.2± 2.7

4.3 Mechanical properties of electrospun nanofibers

The mechanical properties of thick mats of electrospun PAN-CNC composite nanofibers were evaluated. The mechanical analyses were performed using a DMA in linear tensile mode, and the main results are presented in Table 4.3 and Figure 4.5. Generally, the tensile strength of the PAN-CNC composite nanofibers increased for the 10%PAN-10%CNC and 10%PAN-20%CNC in comparison to the 10%PAN nanofibers. The addition of an appropriate amount of CNC inhibit self-aggregation and promote dispersion in the matrix leading to increased strength. Strength and elongation at break has improved because CNCs were expected to be aligned along the tensile

direction during sample elongation and they were able to carry a larger share of the load exerted on the samples. When excess CNC was added, tensile strength and elongation at break decreased. This decrease can be explained by the formation of a rigid network between the CNC that facilitates early crack propagation. Improved mechanicals properties were also reported by Zhang et al. (2015) for Poly(vinylidene fluoride)/Poly(methyl methacrylate) blend reinforced with CNC, Huq et al.(2012) for alginate reinforced with CNC, Lin et al. (2011) for polylactic acid reinforced with CNC, and Zhou et al. (2011) for polyethylene oxide reinforced with CNC.

Table 4.3 Tensile properties of as spun PAN-CNC composite nanofibers. Values are reported as average of two runs ± standard deviation.

Sample	Strength (GPa)	Elongation at break (%)
10%PAN	0.68 ± 0.5	0.6 ± 0.05
10%PAN-10%CNC	1.32 ± 0.2	0.7 ± 0.09
10%PAN-20%CNC	1.81 ± 0.1	0.8 ± 0.05
10%PAN-30%CNC	1.21 ± 0.1	0.7 ± 0.07

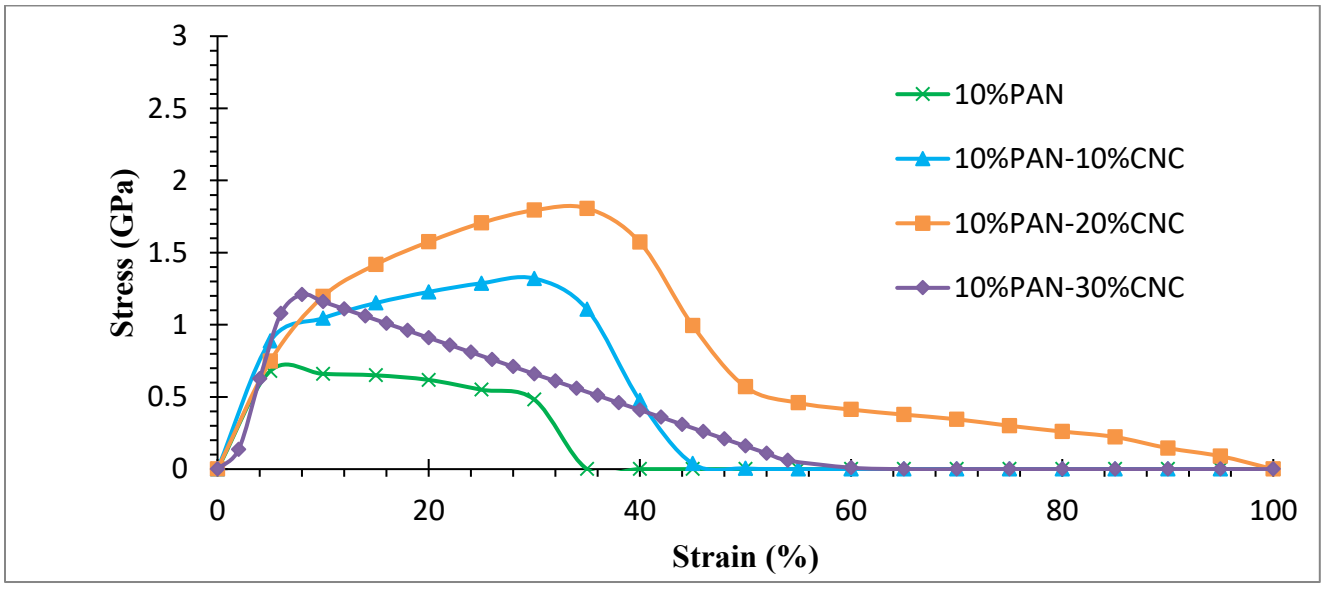

Figure 4.5 Tensile properties of as spun PAN-CNC composite nanofibers

Tensile properties were thus improved upon addition of CNCs. It can be concluded that the observed strength enhancement in CNC-loaded PAN is related to the reinforcing effect of the dispersed phase, via the percolation network held by hydrogen bonds and an increase in mechanical properties resulting from the formation of the network (Peresin et al., 2010).

4.4 Elemental analysis

In this study, the elemental composition is reported for carbonized and activated CnFs, and compared to commercially available activated carbon fiber cloth (ACFC-15) and beaded activated carbon (BAC).

Bulk elemental composition of CnFs at different carbonization temperatures is provided in Table 4.4. The results are based on a triplicate run. Carbon was the most abundant constituent in the samples; hence, CnFs are predominantly carbonaceous. Carbonization removes major non-carbon atoms from the atomic structure and pyrolyzes the fibers into a predominantly carbonaceous residue, thus the increase in carbon content with increasing temperature. The bulk of nitrogen content decreased with carbonization temperature. During the carbonization process, nitrogen continued to be eliminated due to chain fragmentation at high temperature. Sullivan et al. (2012) explained that with increasing temperature, new carbon basal plans forms, and nitrogen is continuously removed during activation. The oxygen content increased with increasing proportion of CNC in the nanofibers, since CNC contains about 50% oxygen per weight, based on molecular weight calculation. Oxygen content appears to be independent of stabilization treatment and carbonization and is reflective of some surface oxidation. In order to balance nitrogen content and porosity, an 800°C activation temperature was chosen as the carbonization temperature since N on the surface of the adsorbents facilitate the adsorption of acidic adsorbates (Song et al., 2008; Bagreev et al., 2004), heavy metals (Yang et al., 2019), and polar adsorbates (Lee et al., 2013).

Table 4.4 Elemental composition of the electrospun PAN-CNC composite nanofibers carbonized at different temperatures. Values are reported as average of three runs ± standard deviation.

Sample	%C	%N	%H	%S	%O*
10%PAN-600	71.03 ± 0.24	21.33 ± 1.03	1.14 ± 0.01	0.00 ± 0.00	6.5 ± 1.05
10%PAN-800	79.29 ± 0.87	10.64 ± 0.98	0.55 ± 0.05	0.00 ± 0.00	9.52 ± 1.16
10%PAN-1000	89.8 ± 0.56	3.14 ± 0.47	0.33 ± 0.03	0.00 ± 0.00	6.73 ± 1.09
10%PAN-10%CNC-600	75.00 ± 0.76	13.97 ±0.63	1.34 ± 0.09	0.00 ± 0.00	9.69 ± 1.69
10%PAN-10%CNC-800	79.68 ± 0.34	9.23 ± 0.87	0.63 ± 0.03	0.00 ± 0.00	10.46 ± 1.24
10%PAN-10%CNC-1000	87.8 ± 0.21	1.76 ± 0.89	0.67 ± 0.02	<0.2 ± 0.00	9.57 ± 1.51
10%PAN-20%CNC-600	79.93 ± 0.98	7.3 ± 1.01	1.44 ± 0.02	<0.2 0.00	11.13 ± 2.09
10%PAN-20%CNC-800	80.05 ± 0.67	5.15 ±1.12	0.56 ±0.09	0.00 ± 0.00	14.24 ± 2.30
10%PAN-20%CNC-1000	81.99 ± 0.76	4.13 ± 0.98	0.34 ± 0.07	0.00 ± 0.00	13.54 ± 1.98
10%PAN-30%CNC-600	80.74 ± 0.97	6.29 ± 1.37	1.17 ± 0.11	0.1 ±0.00	11.7 ± 1.78
10%PAN-30%CNC-800	79.57 ± 1.7	5.21 ± 1.23	0.17 ±0.01	<0.2 ± 0.00	14.85 ± 3.49
10%PAN-30%CNC-1000	82.01 ± 1.2	3.55 ± 0.98	0.52 ± 0.03	0.11 ± 0.00	13.81 ± 2.67

*%O is calculated by % difference

Table 4.5 and 4.6 shows the bulk and the surface elemental composition of ACnFs, ACFC-15, and BAC. The bulk elemental analysis is based on triplicate runs, and the surface elemental analysis is based on duplicate runs. Bulk and surface elemental analysis showed similar results in terms of %atomic of each element, and the only major difference is that carbon content is higher in the bulk than in the surface. ACnFs with different CNC loading are mainly carbonaceous. Bulk

and surface elemental carbon has increased with increasing CNC content except for the 10%PAN-30%CNC. Nitrogen content decreased for the CNC-containing ACnF. Wang et al. (1996) explained that nitrogen groups might act as active sites in the process of activation, and activating agents preferentially interact with the edge or the non-regular parts of the carbon structures, which leads to etching or removal of these parts. The oxygen content increased with the addition of CNC since PAN contains no oxygen in its molecular formula. However, the presence of small amount of oxygen in the 10%PAN sample is reflective of some surface oxidation during stabilization step. ACnFs contained the least amount of C compared to ACFC-15 and BAC, indicating that ACnFs is the least activated. The oxygen content of ACnFs was higher than ACFC and similar to BAC. ACnF contained up to 9 % nitrogen on the surface and in the bulk, which is significantly more than ACFC-15 and BAC. The nitrogen content of ACnF is 5 to 10 times more than in commercial ACFC-15 and BAC. Nitrogen content in ACnF was high when using PAN as Wang et al. (1996) reported. Generally, the presence of nitrogen and oxygen increases the polarity of ACnF and results in increased hydrophilicity compared to that of the ACFC (Wang et al., 1996).

Table 4.5 Bulk elemental analysis of ACnFs, ACFC-15 and BAC. Values are reported as average of three runs ± standard deviation.

Composition	%C	%N	%H	%O*
10%PAN	84.99 ± 0.78	8.87 ± 0.98	<2 ± 0.00	4.14 ± 0.50
10%PAN-10%CNC	87.75 ± 0.66	3.72± 0.43	<2 ± 0.00	6.53 ± 0.87
10%PAN-20%CNC	89.46 ± 0.59	3.27 ± 0.76	<2 ± 0.00	5.27 ± 0.69
10%PAN-30%CNC	87.86 ± 1.09	5.21 ± 1.09	<2 ± 0.00	4.93 ± 0.75
ACFC-15	95.10	0.40	<2	2.50
BAC	91.60	0.00	<2	6.40

*%O is calculated by difference

Table 4.6 Surface elemental analysis (% atomic) of ACnFs, ACFC-15 and BAC using XPS. Values are reported as average of three runs ± standard deviation.

Composition	%C	%N	%O
10%PAN	91.81±1.30	4.11 ± 0.90	4.10 ± 1.00
10%PAN-10%CNC	91.37 ± 1.25	2.64 ± 0.32	5.99 ± 2.10
10%PAN-20%CNC	92.54 ± 0.90	3.14 ± 0.58	4.32 ± 1.02
10%PAN-30%CNC	89.03 ± 0.85	2.98 ± 0.45	7.99 ± 1.50
ACFC	95.40	0.00	4.60
BAC	93.00	0.00	7.00

4.5 Surface area and pore size distribution, adsorption isotherm and kinetics of ACnFs

In addition to surface chemical functional groups, specific surface area and pore structure are important factors that affect the adsorption capacity of carbon adsorbents (Shen et al., 2010). In this study, ACnFs were evaluated for their surface area, pore size distribution, and adsorption capacity for MEK and cyclohexane.

4.5.1 Surface area and pore size distribution

The N_2 adsorption/desorption isotherms at 77 K of PAN-CNC composite nanofibers are shown in Figure 4.5. Based on their shapes, the isotherms for 10%PAN, 10%PAN-10%CNC, 10%PAN-20%CNC, ACFC-15, and BAC follow type I isotherm, characterized by an abrupt knee at low relative pressure, P/P_0, followed by a slight increase in the nitrogen uptake at high relative pressure indicating that the samples are mainly composed of micropores. Gregg and Sing (1982) describe a type I isotherm as representative of gas adsorption in microporous adsorbents. The sharp

rise in adsorption capacity at low relative pressure corresponds to the micropore filling, and the flat plateau in the higher pressure range corresponds to the absence of larger pores in the system. This mechanism, they note, is due to the pores being so narrow that they cannot accommodate more than a single molecular layer. From the upward sloped center section of its N_2 adsorption isotherm, 10%PAN, 10%PAN-10%CNC, and 10%PAN-20%CNC can qualitatively be seen to have a wider pore distribution that includes mesopores. The adsorption isotherms for the ACFC-15 and BAC plateaued more rapidly, showing slight mesoporosity in comparison to other ACnFs. Li et al. (1998) showed similar results for ACFC-15, and Wang et al. (2006) for PAN-based ACnFs.

On the other hand, the shape of 10%PAN-30%CNC isotherm exhibited some features of type IV according to the International union of pure and applied chemistry (IUPAC) classification indicating the presence of capillary condensation as the relative pressure approaches unity. The initial part of the Type IV isotherm is attributed to monolayer-multilayer adsorption followed by a sharp step at high relative pressures indicative of capillary condensation within mesopores (Gregg and Sing, 1982).

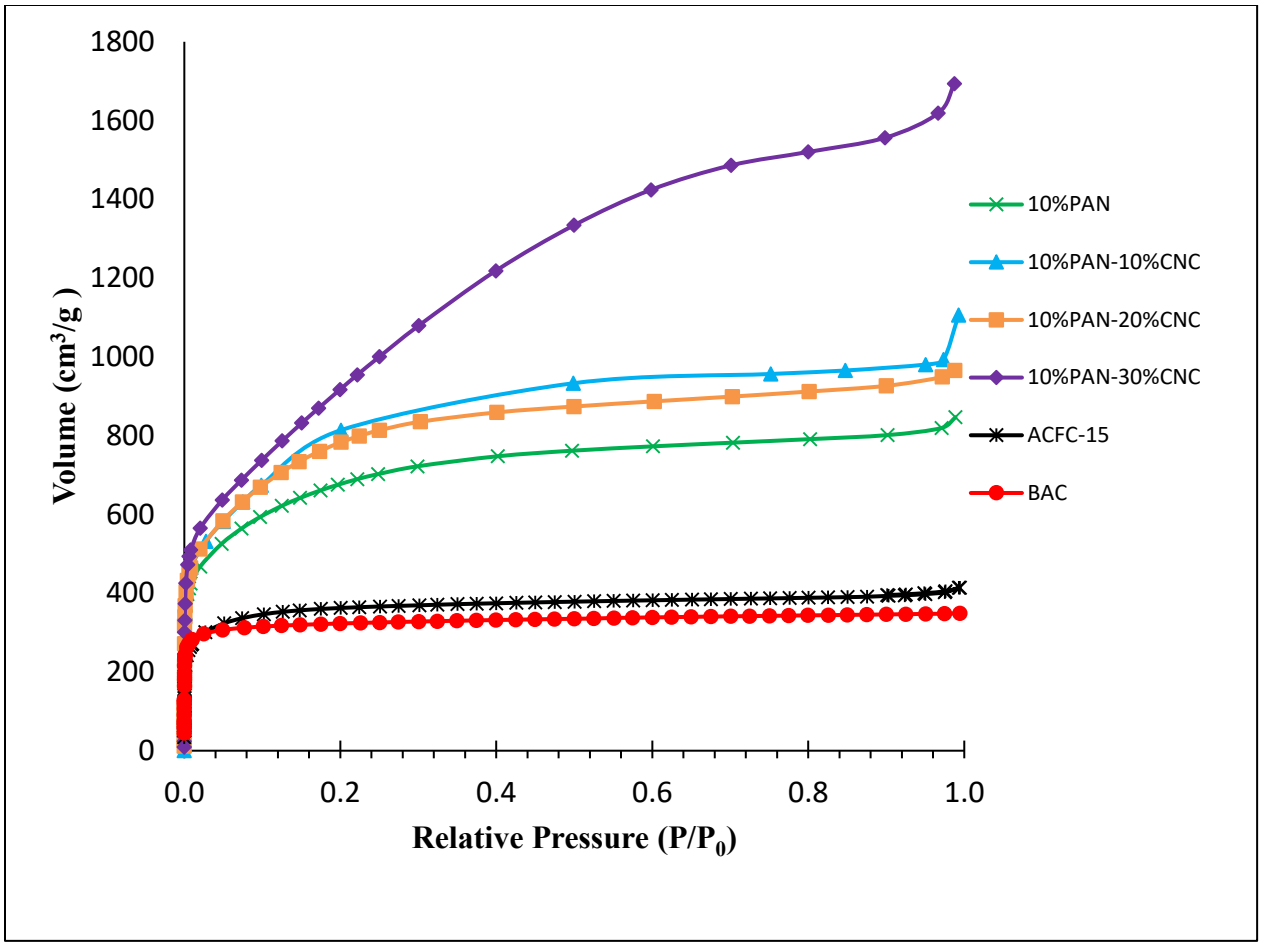

Figure 4.6 N_2 adsorption isotherm at 77K of ACnFs, ACFC-15 and BAC

Specific surface area and pore size distribution results are summarized in Table 4.7. The obtained results are based on a duplicate run of the samples. Among the ACnFs, the most developed porosity corresponded to the 10%PAN-30%CNC sample. The surface area and the total pore volume increased with increasing the CNC content in ACnFs. ACnFs showed higher surface area and total pore volume but a lower microporosity compared to ACFC-15 and BAC.

Table 4.7 Surface area and pore volume of ACnFs, ACFC-15 and BAC. Values are reported as average of two runs ± standard deviation.

Sample	Micropore volume (cm^3/g)	Total pore volume (cm^3/g)	Microporosity (%)	Average micropore width (Å)	Surface area (m^2/g)
10%PAN	0.96 ± 0.07	1.27 ± 0.08	75.6 ± 0.05	10.65 ± 0.10	2429 ± 97.7
10%PAN-10%CNC	1.15 ± 0.10	1.53 ± 0.09	75.1 ± 0.02	11.01 ± 0.04	2853 ± 110.3
10%PAN-20%CNC	1.12 ± 0.09	1.49 ± 0.07	75.2 ± 0.03	10.81 ±0.09	2836 ± 134.5
10%PAN-30%CNC	1.04 ± 0.04	2.62 ± 0.01	39.7 ± 0.02	11.02 ± 0.04	3497 ± 80.5
ACFC-15	0.45 ± 0.31	0.47 ± 0.09	95.7 ± 0.43	7.7 ± 0.1	1215 ± 80.9
BAC	0.5 ± 0.22	0.57 ± 0.10	87.8 ± 0.24	11.38 ± 0.2	1371 ±120.4

Pore size distribution of the ACnF, ACFC-15, and BAC are presented in Figure 4.6. 10%PAN-30%CNC showed high mesoporosity indicative of a type IV adsorption isotherm. 10%PAN, 10%PAN-10%CNC, 10%PAN-20%CNC showed a slight mesoporosity, and ACFC and BAC showed a high microporosity. The surface area is strongly dependent on the pore size distribution as explained by Saha and Grappe (2017). ACnFs with surface area below 3,000 m^2/g present a narrow pore size distribution, with low mesoporosity, whereas ACnFs with surface area higher than 3,000 m^2/g have a broader pore size distribution with wider pores size distribution. In

conclusion, the addition of CNC into the ACnFs has increased surface area and has contributed to higher mesoporosity.

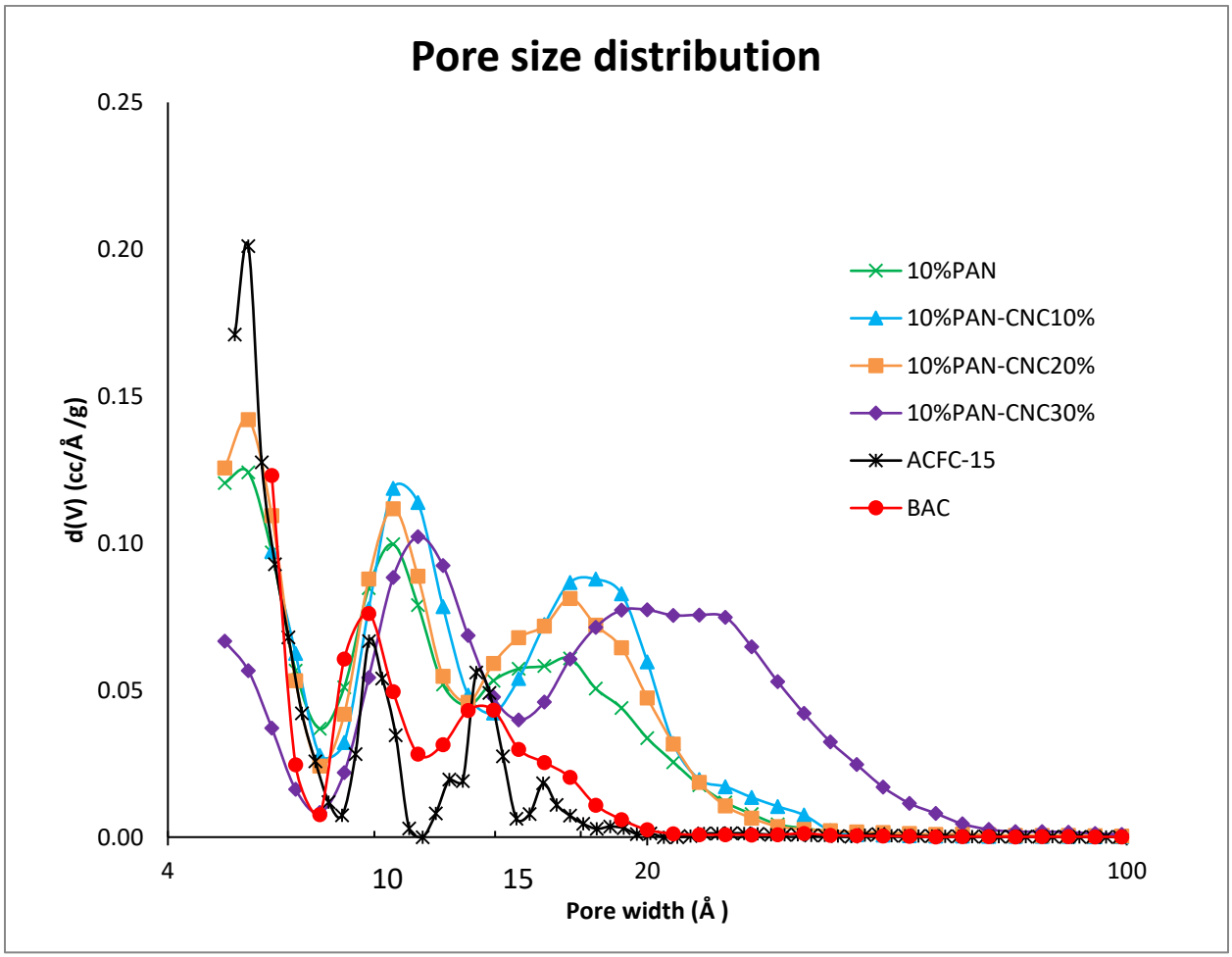

Figure 4.7 Pore size distribution of ACnFs, ACFC-15, and BAC

4.5.2 Gravimetric adsorption isotherms

The adsorption capacity of ACnFs for volatile organic compounds (VOCs) were measured and compared to that of commercially available ACFC-15 and BAC. MEK and cyclohexane were chosen as adsorbates based on their similar chemical and physical properties, as shown in Table 4.8. Samples were exposed to MEK and cyclohexane carried by a N_2 stream at room temperature

and their adsorption capacities were measured following the procedures explained in the experimental section.

Table 4.8 Physical and chemical characteristics of MEK and cyclohexane

Adsorbate	Formula	Molecular weight (g/mol)	Boiling point (°C) at 1 atm	Vapor pressure at 22 °C (mmHg)	Kinetic diameter (Å)	Density at 22°C (g/mL)	Heat of vaporization (KJ/mol)
MEK	$CH_3COC_2H_5$	72.11	79.6	71	5.25[a]	0.81[a]	34.1[c]
Cyclohexane	C_6H_{12}	84.16	80.74	78	5.80[b]	0.78[b]	37.7[c]

Note: [a]Lee et al.,2008; [b]Magalhães et al., 1998; [c]Weast,1984

MEK and cyclohexane adsorption isotherms for ACnFs, ACFC-15, and BAC are described in Figures 4.7 and 4.8, respectively (detailed adsorption data are presented in Appendix A and B). Adsorption isotherm for all the adsorbent were type I according to the IUPAC classification, except for the 10%PAN-30%CNC which exhibited some features of type IV as shown previously. These results showed that ACnFs containing CNC had higher adsorption capacity compared to PAN only ACnF. The 10%PAN-30%CNC sample had the highest adsorption capacity because it has the highest total pore volume and largest surface area. MEK adsorption capacity on ACnFs is higher than cyclohexane. This could be because the methyl group (-CH3) of MEK in its chemical structure, caused π-π interaction between VOCs and the electrospun composite nanofiber mats and led to an increase in the binding energy thus increased adsorption capacity. In addition, the presence of high nitrogen concentration on the surface and some oxygen functionalities resulted in enhanced adsorption of MEK (as in Ge & Choi, 2017; Ge et al., 2018; Ge et al., 2016). Besides that, the kinetic diameter of MEK (5.25 Å) is smaller than cyclohexane (5.80 Å) which facilitates the passage of MEK into narrow adsorption sites.

ACnFs possess higher adsorption capacity than ACFC-15 and BAC as shown in Figure 4.7 and 4.8. The large capacity of the ACnFs could be explained first by the high total pore volume.

Second, by the interactions of the adsorbates with a number of different surface functional groups (N and O) present in high concentration on the large surface area as shown in the elemental composition section. Lee et al. (2013) concluded that the adsorption capacity of a porous carbon material is determined mainly by the pore volume, surface area and the presence of functional groups on the adsorbent. Similarly, Lee et al. (2010) found that toluene adsorption on ACnF is much higher than ACF in both dry and humid conditions. In addition, Song et al. (2007) showed that the higher the N content in the CF, the higher its adsorption capacity for formaldehyde removal. It should be noted that, at low adsorbate concentration, ACnF, ACFC, and BAC perform quite similarly while at high adsorbate concentration, the difference in adsorption capacity is remarkable (Figure 4.7 and 4.8). This behavior is expected since at low adsorbate concentration; adsorption is controlled by adsorbate-adsorbent interaction which are favored in adsorbents with narrower pores as in ACFC and BAC. However, at high concentrations, the adsorption capacity of ACnFs is higher than ACFC and BAC since it is controlled by the total pore volume of the adsorbent and adsorbate–adsorbate interaction and not only adsorbate–adsorbent interaction, as explained by Sullivan et al. (2012). In addition, ACnFs possess high mesoporosity particularly for the 10%PAN-30%CNC. The presence of mesopores and macropores is beneficial as explained by Gil et al. (2014). Those pores provide the necessary channels for adsorbates transport and are filled with adsorbates at high relative pressure. Besides the pore structure, surface chemical functional groups such as oxygen and nitrogen of carbon materials may act as active sites and be responsible for their high adsorption capacity (Chiang et al., 2002; Li et al., 2011).

In conclusion, for any adsorbent and at low RP, large specific surface area and micropore volume usually indicate superior adsorption performance because surface area provides the sites for adsorption processes. In addition, pore size distribution is important for adsorption capacity. In general, micropores provide principal adsorption sites, while the mesopores enhance the intra-particle diffusion and shorten the adsorption time. ACnFs have higher pore volume and higher mesoporosity, hence their superior adsorption capacity over ACFC and BAC at high RP. Finally, the presence of CNC in ACnFs, had increased surface area and pore volume leading to higher adsorption capacity compared to only PAN ACnFs.

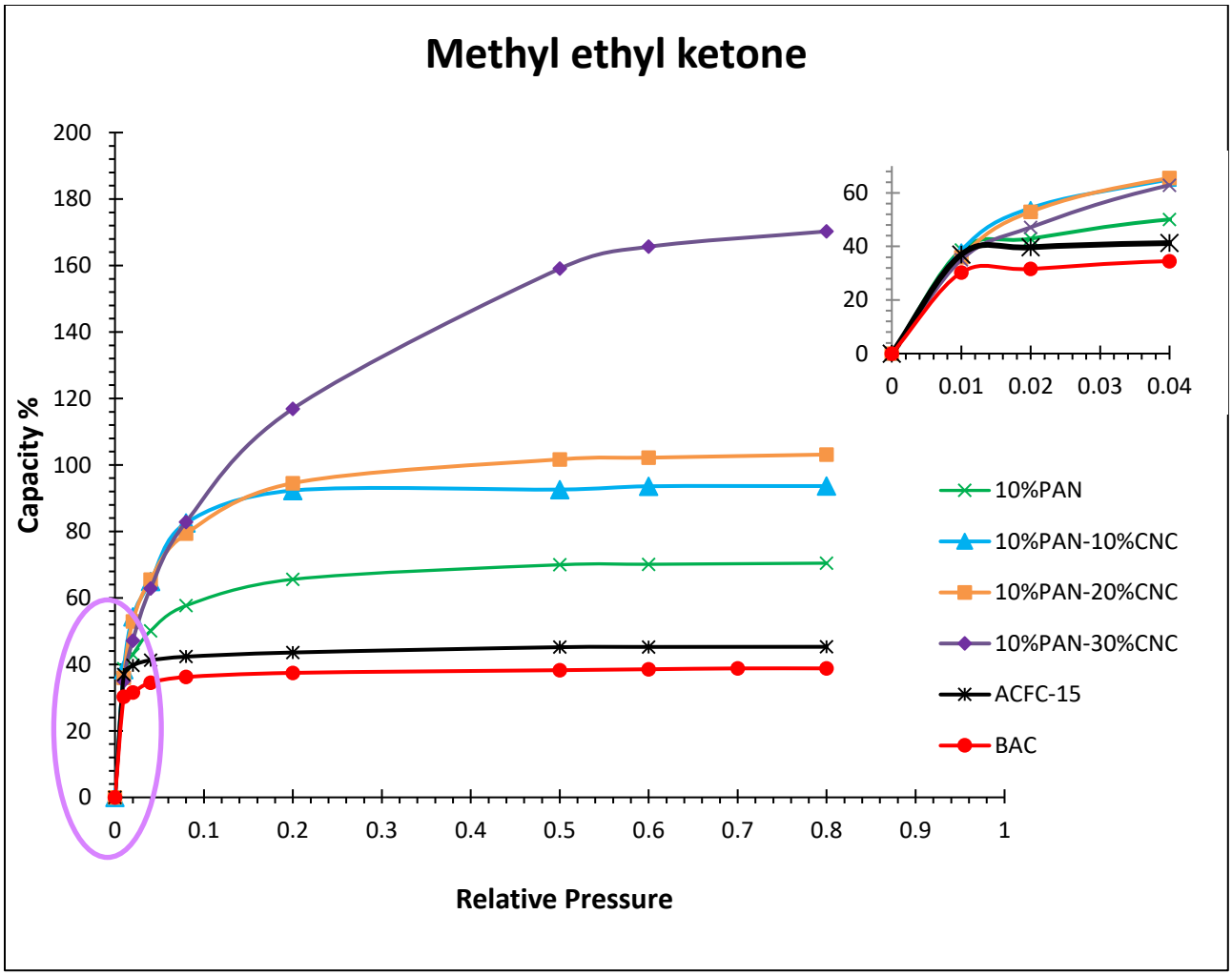

Figure 4.8 MEK adsorption isotherm on ACnFs, ACFC-15, and BAC.

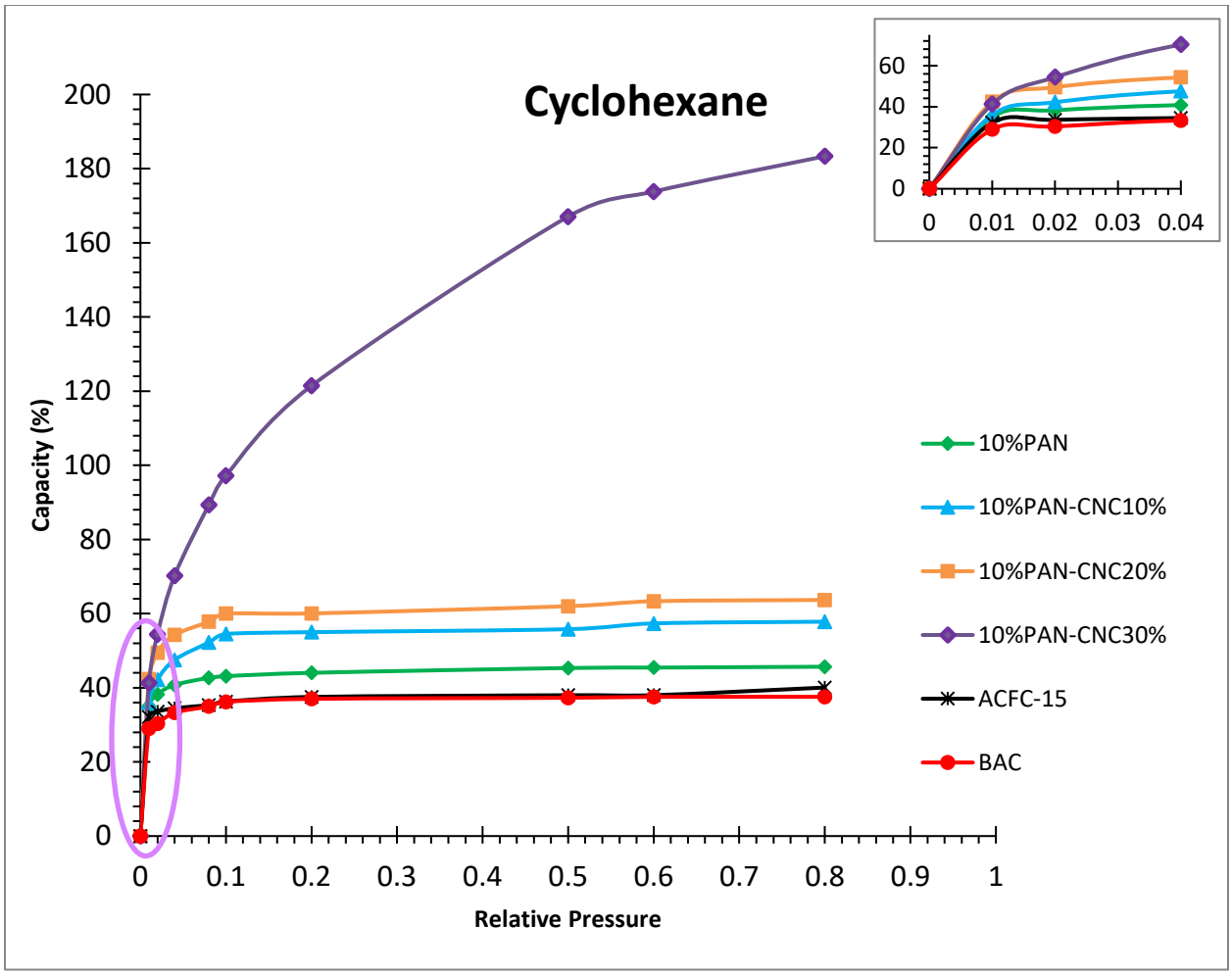

Figure 4.9 Cyclohexane adsorption isotherm on ACnFs, ACFC-15, and BAC.

4.5.3 Kinetics of adsorption

Kinetics of MEK adsorption on ACnFs, ACFC-15, and BAC are presented in Figure 4.10. The rate constant K values were the average of two measurements. For ACnFs with different CNC content, 10%PAN-30%CNC showed the highest adsorption rate constant. Increasing the amount of CNC, increased the adsorption rate constant. The higher amount of cellulose nanoparticles led to higher number of nanoparticles in the matrix as well as higher number of mesopores resulting in faster kinetics. In addition, the incorporation of CNC inside the nanofibers matrix has decreased average size diameter of ACnFs resulting in decrease in the internal mass transfer thus the increase

in the adsorption rate constant. ACnFs demonstrated the fastest rate of adsorption among the tested adsorbents. Rate of MEK adsorption for ACnF was nearly twice that of ACFC-15 and about 20 times faster than BAC as shown in Figure 4.10. In general, the rate of adsorption is influenced by the adsorbent particle size, pore size distribution, and the quantity and accessibility of micropores. Wang et al. (2015) found that the diffusion rate constants of VOCs in ordered mesoporous carbon are almost twice that in microporous AC. Thus, the adsorption rates of VOCs in mesopores are faster than that in micropore due to the higher intra-particle diffusion rate. The combination of filamentous structure of ACnFs and the presence of mesopores has permitted a very efficient contact between the adsorbate and the adsorbent surface as explained by Lordgooei et al. (1996). Sullivan et al. (2012) explained that the nano-size fibers of ACnF with a high external surface to volume ratio likely facilitate both internal and external mass transfer. Internal mass transfer time is reduced since the mean distance the adsorbate must travel is shorter. The high external surface area provides better access to the adsorbent's internal micropores. The kinetics of MEK adsorption results are in accordance with ethane adsorption kinetics for ACnFs, ACFC, and GAC done by Sullivan et al. (2012). Generally, ACFs have larger diameter than ACnFs resulting in deeper pores than ACnFs. Shallow pores are developed on carbon fiber with small diameter thus resulting in superior adsorption capability. Therefore, ACnFs had faster kinetics than ACFC. As a conclusion, the fast kinetics observed for ACnF are advantageous for adsorption processes in general, and can result in improved adsorbent utilization.

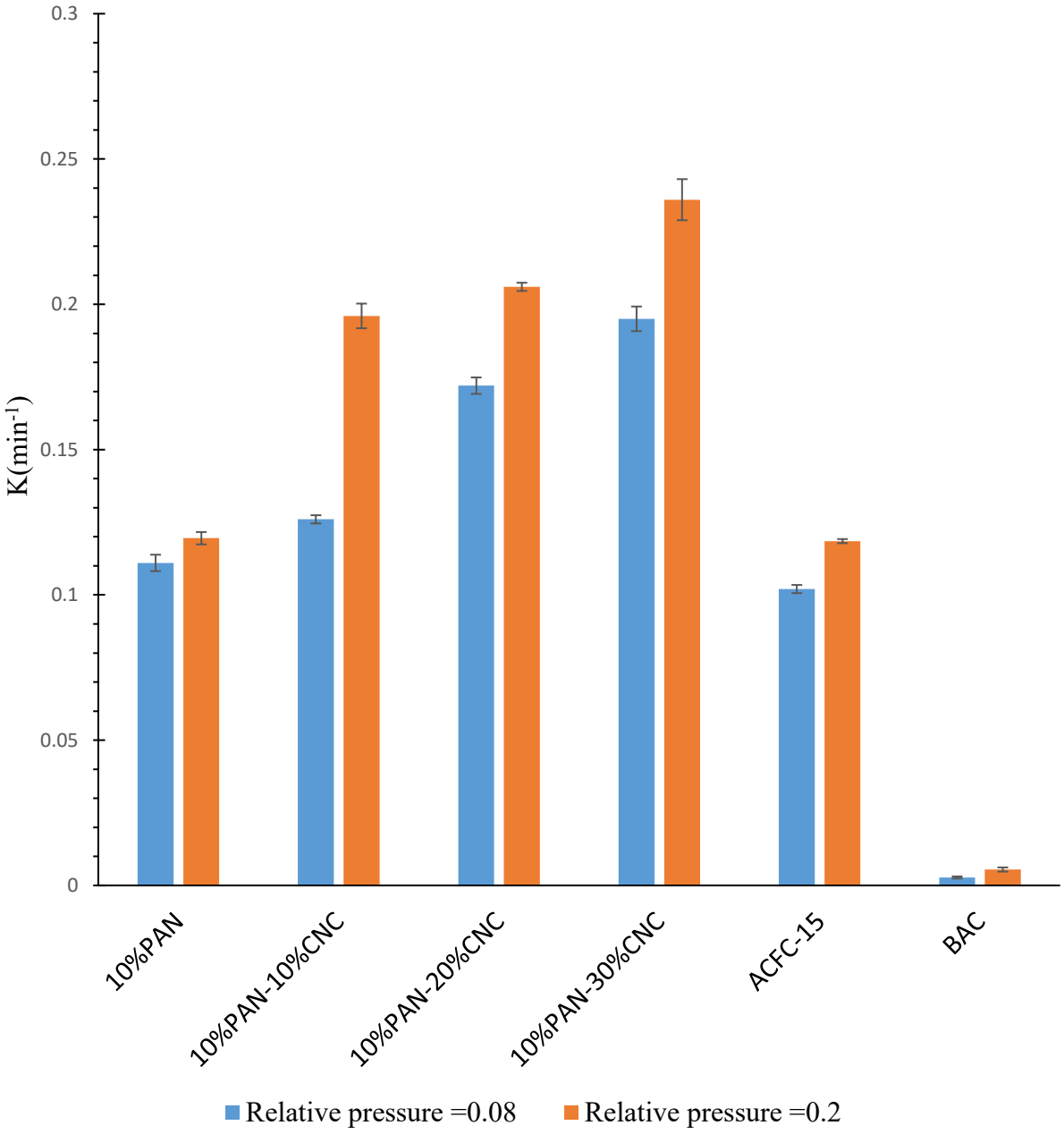

Figure 4.10 Adsorption rate constant of ACnFs, ACFC-15, and BAC. Error bars indicate the standard deviation around the average of two sets of data.

Chapter 5 Conclusions and Recommendations

5.1 Summary

This study consisted of two major components: investigating the effect of CNC addition on carbon nanofibers properties, and the adsorption properties of ACnFs. PAN polymers reinforced with CNC were electrospun into very thin nanofibers. Factors related to the electrospinning process (solution viscosity, polymer concentration) were optimized to obtain uniform nanofibers. The obtained electrospun composite nanofibers were successfully carbonized and chemically activated using KOH. CNC-reinforced nanofiber mats were assessed for their morphology, thermal stability, chemical properties, and mechanical properties. The activated reinforced nanofiber mats were tested for their adsorption and pore size distribution as well as adsorption kinetics. Finally, their performance was compared to commercially available ACFC and BAC.

5.2 Conclusions

The main conclusions from incorporating CNC into carbon nanofibers are summarized as follow:

- Average diameter of the electrospun nanofibers has decreased in presence of CNC. CNC external surface possess negatively charged sulphate groups which may increase solution conductivity. Upon increasing solution conductivity more extensive filament stretching during jet whipping occurs and leasto decrease in electrospun nanofibers diameter.
- Increase in thermal stability for the nanocomposite nanofibers in comparison to neat nanofibers except for the 10%PAN-30%CNC sample. The influence of CNCs on the thermal behavior of PAN/CNC nanocomposites could be explained by the interactions between the hydroxyl groups of CNCs and the nitril groups of PAN.
- Tensile strength of CNC reinforced composites increased with CNC content initially, and then decreased when 30% CNC was added. The maximum strength was found to occur at 20 wt% CNC fiber content. The increase was attributed to strong fiber-matrix interfacial bonding. On the other hand, high CNC content resulted in fiber agglomeration, which caused lower strain-at-failure for PAN/CNC composites. Thus, the decrease in tensile strength for the 10%PAN-30%CNC.

- ACnFs are predominantly carbonaceous and have high nitrogen content (5-10%). This is due to the use of PAN as precursor when preparing the ACnFs. Generally, these levels of nitrogen increase the polarity of the ACnFs and are expected to enhance adsorption capacity for polar, heavy metals, and acidic adsorbates.

The main conclusions from the adsorption isotherm and kinetics of ACnFs are summarized as follow:

- Reinforced ACnFs exhibited type I isotherm except for the 10%PAN-30%CNC. The shape of 10%PAN-CAN30% isotherm is considered type IV. Among the ACnFs, the most developed porosity corresponded to the 10%PAN-30%CNC sample.
- The specific surface area and total pore volume of ACnFs increased as CNC content increased. The microporosity of 10%PAN, 10%PAN-10%CNC, 10%PAN-20%CNC was around 75%, and 40% for 10%PAN-30%CNC, with a 43% mesoporosity.
- The presence of CNC in ACnFs resulted in increased surface area and pore volume leading to higher adsorption capacity and faster kinetics compared to neat PAN ACnFs.
- ACnFs had superior adsorption capacity over commercially available ACFC and BAC, due to its larger pore volume and higher mesoporosity that enhances inter-particle diffusion.
- The superior kinetics of ACnFs are due to their filamentous structure, which in combination of presence of mesopores permit a very efficient contact between the adsorbate and adsorbent surface.

5.3 Future applications and recommendations

This research investigated and developed ACnFs for adsorption purposes. Based on the obtained results and conclusions, the following recommendations can be made for future research:

- Many VOC-laden gas streams contain mixtures of VOCs (polar and non-polar) together-with water vapor, which compete for the available adsorption sites. The ACnFs

developed in this research could be further tested to account for more than one VOC and a VOC-water vapor mixture.

- ACnF's outstanding properties, high porosity, large specific surface area, and low density with uniform fiber size, may facilitate the development of improved air purification devices such as respirators and filter systems.
- Furthermore, incorporating different ingredients like inorganic compounds: Ag, Cu, CNTs, and TiO_2 is possible to prepare nanofibers with unique properties such as antibacterial and photocatalytic.

Bibliography

Aktaş, Ö, & Çeçen, F. (2006). Effect of type of carbon activation on adsorption and its reversibility. *Journal of Chemical Technology & Biotechnology, 81*(1), 94-101.

Alexei Lapkin, Lucy Joyce, & Barry Crittenden. (2004). Framework for evaluating the "greenness" of chemical processes: Case studies for a novel VOC recovery technology. *Environmental Science & Technology, 38*(21), 5815-5823.

Álvarez, P. M., García-Araya, J. F., Beltrán, F. J., Masa, F. J., & Medina, F. (2005). Ozonation of activated carbons: Effect on the adsorption of selected phenolic compounds from aqueous solutions. *Journal of Colloid and Interface Science, 283*(2), 503-512.

Arshad, S. N., Naraghi, M., & Chasiotis, I. (2011). Strong carbon nanofibers from electrospun polyacrylonitrile. *Carbon, 49*(5), 1710-1719.

Ashammakhi, N., Wimpenny, I., Nikkola, L., & Yang, J. (2009). Electrospinning: Methods and development of biodegradable nanofibres for drug release. *Journal of Biomedical Nanotechnology*, *5*(1), 1-19.

Astashkina, O., Bogdan, N., Lysenko, A., & Kuvaeva, E. (2008). Production of activated carbon fibres by solid-phase (chemical) activation. *Fibre Chemistry, 40*(3), 179-185.

Azizian, S. (2004). Kinetic models of sorption: A theoretical analysis. *Journal of Colloid and Interface Science, 276*(1), 47-52.

Bae, H., Haider, A., Selim, K., Kang, D., Kim, E., & Kang, I. (2013). Fabrication of highly porous PMMA electrospun fibers and their application in the removal of phenol and iodine. *Journal of Polymer Research, 20*(7), 1-7.

Baker, S. E., Tse, K., Lee, C., & Hamers, R. J. (2006). Fabrication and characterization of vertically aligned carbon nanofiber electrodes for biosensing applications. *Diamond & Related Materials, 15*(2), 433-439.

Bansal, R. C., & Goyal, M. (2005). *Activated carbon adsorption*. Boca Raton: Taylor & Francis.

Bagreev, A., Angel Menendez, J., Dukhno, I., Tarasenko, Y., & Bandosz, T. J. (2004). Bituminous coal-based activated carbons modified with nitrogen as adsorbents of hydrogen sulfide. *Carbon, 42*(3), 469-476.

Bhardwaj, N., & Kundu, S. C. (2010). Electrospinning: A fascinating fiber fabrication technique. *Biotechnology Advances, 28*(3), 325-347.

Billemont, P., Coasne, B., & De Weireld, G. (2013). Adsorption of carbon dioxide, methane, and their mixtures in porous carbons: Effect of surface chemistry, water content, and pore disorder. *Langmuir: The ACS Journal of Surfaces and Colloids, 29*(10), 3328-3338.

Calvete, T., Lima, E. C., Cardoso, N. F., Dias, S. L. P., & Pavan, F. A. (2009). Application of carbon adsorbents prepared from the brazilian pine-fruit-shell for the removal of procion red MX 3B from aqueous solution—Kinetic, equilibrium, and thermodynamic studies. *Chemical Engineering Journal, 155*(3), 627-636.

Cao, X., Habibi, Y., Magalhães, W., Rojas, O., & Lucia, L. (2011). Cellulose nanocrystals-based nanocomposites: Fruits of a novel biomass research and teaching platform. *Current Science, 100*(8), 1172-1176.

Chang, H., Luo, J., Liu, H. C., Zhang, S., Park, J. G., Liang, R., & Kumar, S. (2019). Carbon fibers from polyacrylonitrile/cellulose nanocrystal nanocomposite fibers. *Carbon*, *145*, 764-771.

Chen, J. C., & Harrison, I. R. (2002). Modification of polyacrylonitrile (PAN) carbon fiber precursor via post-spinning plasticization and stretching in dimethyl formamide (DMF). *Carbon, 40*(1), 25-45.

Chiang, P. C., Chiang, H., & Huang, C. P. (2002). The surface characteristics of activated carbon as affected by ozone and alkaline treatment. *Chemosphere, 47*(3), 257-265.

Chiu, K., & Ng, D. H. L. (2012). Synthesis and characterization of cotton-made activated carbon fiber and its adsorption of methylene blue in water treatment. *Biomass and Bioenergy, 46*, 102-110.

Chuang, C. L., Chiang, P. C., & Chang, E. E. (2003). Modeling VOCs adsorption onto activated carbon. *Chemosphere, 53*(1), 17-27.

Chung, D. (2004). Electrical applications of carbon materials. *Journal of Materials Science, 39*(8), 2645-2661.

Chung, D. D. L. (2012). Carbon materials for structural self-sensing, electromagnetic shielding and thermal interfacing. *Carbon, 50*(9), 3342-3353.

Dąbrowski, A., Podkościelny, P., Hubicki, Z., & Barczak, M. (2005). Adsorption of phenolic compounds by activated carbon—a critical review. *Chemosphere, 58*(8), 1049-1070.

Das, D., Gaur, V., & Verma, N. (2004). Removal of volatile organic compound by activated carbon fiber. *Carbon, 42*(14), 2949-2962.

Deitzel, J. M., Kleinmeyer, J. D., Hirvonen, J. K., & Beck Tan, N. C. (2001). Controlled deposition of electrospun poly(ethylene oxide) fibers. *Polymer, 42*(19), 8163-8170.

Demir, M. M., Yilgor, I., Yilgor, E., & Erman, B. (2002). Electrospinning of polyurethane fibers. *Polymer, 43*(11), 3303-3309.

Díaz, E., Ordóñez, S., & Vega, A. (2007). Adsorption of volatile organic compounds onto carbon nanotubes, carbon nanofibers, and high-surface-area graphites. *Journal of Colloid and Interface Science, 305*(1), 7-16.

Díez, N., Álvarez, P., Granda, M., Blanco, C., Santamaría, R., & Menéndez, R. (2015). A novel approach for the production of chemically activated carbon fibers. *Chemical Engineering Journal, 260*, 463-468.

Dong, H., Strawhecker, K. E., Snyder, J. F., Orlicki, J. A., Reiner, R. S., & Rudie, A. W. (2012). Cellulose nanocrystals as a reinforcing material for electrospun poly(methyl methacrylate) fibers: Formation, properties and nanomechanical characterization. *Carbohydrate Polymers, 87*(4), 2488-2495.

Dwivedi, P., Gaur, V., Sharma, A., & Verma, N. (2004). Comparative study of removal of volatile organic compounds by cryogenic condensation and adsorption by activated carbon fiber. *Separation and Purification Technology, 39*(1), 23-37.

Edgar, K. J., Buchanan, C. M., Debenham, J. S., Rundquist, P. A., Seiler, B. D., Shelton, M. C., & Tindall, D. (2001). Advances in cellulose ester performance and application. *Progress in Polymer Science, 26*(9), 1605-1688.

Efremenko, I., & Sheintuch, M. (2006). Predicting solute adsorption on activated carbon: Phenol. *Langmui : The ACS Journal of Surfaces and Colloids, 22*(8), 3614-3621.

Eichhorn, S., Dufresne, A., Aranguren, M., Marcovich, N., Capadona, J., Rowan, S., Weder C, Thielemans W, Roman M, Renneckar S, Peijs, T. (2010). Review: Current international research into cellulose nanofibres and nanocomposites. *Journal of Materials Science, 45*(1), 1-33.

Erich, K., Sabu, T., & Kajal, G. (2018). Electrical spinning to electrospinning: A brief history. *Electrospinning - from basic research to commercialization* (pp. 1) Royal Society of Chemistry.

Evtyugina, M. G., Pio, C., Nunes, T., Pinho, P. G., & Costa, C. S. (2007). Photochemical ozone formation at portugal west coast under sea breeze conditions as assessed by master chemical mechanism model. *Atmospheric Environment, 41*(10), 2171-2182.

Fukushima, M., Zhou, Y., Miyazaki, H., Yoshizawa, Y., Hirao, K., Iwamoto, Y., Yamazaki S, Nagano, T. (2006). Microstructural characterization of porous silicon carbide membrane support with and without alumina additive. *Journal of the American Ceramic Society, 89*(5), 1523-1529.

Gao, X., Sadasivuni, K., Kim, H., Min, S., & Kim, J. (2015). Designing pH-responsive and dielectric hydrogels from cellulose nanocrystals. *Journal of Chemical Sciences, 127*(6), 1119-1125.

Ge, J. C., & Choi, N. J. (2017). Fabrication of functional polyurethane/rare earth nanocomposite membranes by electrospinning and its VOCs absorption capacity from air. *Nanomaterials (Basel, Switzerland), 7*(3), 60.

Ge, J. C., Wang, Z. J., Kim, M. S., & Choi, N. J. (2018). VOCs air pollutant cleaning with polyacrylonitrile/fly ash nanocomposite electrospun nanofibrous membranes. *IOP Conference Series: Materials Science and Engineering, 301*, 12036.

Gil, R. R., Ruiz, B., Lozano, M. S., Martín, M. J., & Fuente, E. (2014). VOCs removal by adsorption onto activated carbons from biocollagenic wastes of vegetable tanning. *Chemical Engineering Journal, 245*, 80-88.

Gregg-S-J, & Sing-K-S-W. (1982). *Adsorption, surface area and porosity* (2nd ed.)

Gupta, V. K., & Verma, N. (2002). Removal of volatile organic compounds by cryogenic condensation followed by adsorption. *Chemical Engineering Science, 57*(14), 2679-2696.

Habibi, Y., Lucia, L. A., & Rojas, O.J. (2010). Cellulose nanocrystals: Chemistry, self-assembly, and applications. *Chemical Reviews, 110*(6), 3479-3500.

Haider, S., Haider, A., & Kang, I. (2018). A comprehensive review summarizing the effect of electrospinning parameters and potential applications of nanofibers in biomedical and biotechnology. *Arabian Journal of Chemistry, 11*(8), 1165-1188.

Hamad, W. Y. (2017). *Cellulose nanocrystals* (1st ed.). GB: Wiley.

Hou, H., Ge, J. J., Zeng, J., Li, Q., Reneker, D. H., Greiner, A., & Cheng, S. Z. D. (2005). Electrospun polyacrylonitrile nanofibers containing a high concentration of well-aligned multiwall carbon nanotubes. *Chemistry of Materials, 17*(5), 967-973.

Huq, T., Salmieri, S., Khan, R. A., Khan, A., Le Tien, C., Riedl, B., Fraschini C, Bouchard J, Uribe-Calderon J, Kamal MR, Lacroix, M. (2012). Nanocrystalline cellulose (NCC) reinforced alginate based biodegradable nanocomposite film. *Carbohydrate Polymers, 90*(4), 1757-1763.

Hussain, F., Hojjati, M., Okamoto, M., & Gorga, R. E. (2006). Review article: Polymer-matrix nanocomposites, processing, manufacturing, and application: An overview. *Journal of Composite Materials, 40*(17), 1511-1575.

Ingavle, G. C., & Leach, J. K. (2014). Advancements in electrospinning of polymeric nanofibrous scaffolds for tissue engineering. *Tissue Engineering Part B: Reviews, 20*(4), 277-293.

Jaroniec, M., Gilpin, R. K., Kaneko, K., & Choma, J. (1991). Evaluation of energetic heterogeneity and microporosity of activated carbon fibers on the basis of gas adsorption isotherms. *American Chemical Society, 7*(11), 2719-2722.

Ji, L., Yao, Y., Toprakci, O., Lin, Z., Liang, Y., Shi, Q., Medford, AJ., Millns, CR.,

Ju, Y., & Oh, G. (2017). Behavior of toluene adsorption on activated carbon nanofibers prepared by electrospinning of a polyacrylonitrile-cellulose acetate blending solution. *Korean Journal of Chemical Engineering, 34*(10), 2731-2737.

Jun Cong Ge, Jeong Hyeon Kim, & Nag Jung Choi. (2016). Electrospun polyurethane/loess powder hybrids and their absorption of volatile organic compounds. *Advances in Materials Science and Engineering, 2016*, 1-8.

Kai, D., Liow, S. S., & Loh, X. J. (2014). Biodegradable polymers for electrospinning: Towards biomedical applications. *Materials Science & Engineering. C, Materials for Biological Applications, 45*, 659-670.

Kawasaki, N., Kinoshita, H., Oue, T., Nakamura, T., & Tanada, S. (2004). Study on adsorption kinetic of aromatic hydrocarbons onto activated carbon in gaseous flow method. *Journal of Colloid and Interface Science, 275*(1), 40-43.

Kim, J., & Reneker, D. H. (1999). Polybenzimidazole nanofiber produced by electrospinning. *Polymer Engineering & Science, 39*(5), 849-854.

Ko, T., Chiranairadul, P., Lu, C., & Lin, C. (1992). The effects of activation by carbon dioxide on the mechanical properties and structure of PAN-based activated carbon fibers. *Carbon, 30*(4), 647-655.

Kunowsky, M., Suárez-García, F., Cazorla-Amorós, D., & Linares-Solano, A. (2008). Synthesis of activated carbon fibers for High-Pressure hydrogen storage. *Materials innovations in an emerging hydrogen economy*, 69-75.

Kvien, I., Tanem, B. S., & Oksman, K. (2005). Characterization of cellulose whiskers and their nanocomposites by atomic force and electron microscopy. *Biomacromolecules, 6*(6), 3160-3165.

Larrondo, L., & St. John Manley, R. (1981). Electrostatic fiber spinning from polymer melts. II. examination of the flow field in an electrically driven jet. *Journal of Polymer Science: Polymer Physics Edition. 19(6)*, 921-932.

Lee, H., Kang, H., An, K., Kim, H., & Kim, B. (2013). Comparative studies of porous carbon nanofibers by various activation methods. *Carbon Letters, 14*(3), 180-185.

Lee, K. J., Miyawaki, J., Shiratori, N., Yoon, S., & Jang, J. (2013). Toward an effective adsorbent for polar pollutants: Formaldehyde adsorption by activated carbon. *Journal of Hazardous Materials, 260*, 82-88.

Lee, K. J., Shiratori, N., Lee, G. H., Miyawaki, J., Mochida, I., Yoon, S., & Jang, J. (2010). Activated carbon nanofiber produced from electrospun polyacrylonitrile nanofiber as a highly efficient formaldehyde adsorbent.*Carbon. 48(15)*, 4248-4255.

Lee, S., Cheon, J., Park, H., & Lee, M. (2008). Adsorption characteristics of binary vapors among acetone, MEK, benzene, and toluene. *Korean Journal of Chemical Engineering, 25*(5), 1154-1159.

Lee, Y. J., Kim, J. H., Kim, J. S., Lee, D. B., Lee, J. C., Chung, Y. J., & Lim, Y. S. (2004). Fabrication of activated carbon fibers from stabilized PAN-based fibers by KOH. *Materials Science Forum,* 449-452:217-20.

Li, L., Liu, J., & Liu, S. (2011). Surface modification of coconut shell based activated carbon for the improvement of hydrophobic VOC removal. *Journal of Hazardous Materials, 192*(2), 683-690.

Li, Z., Kruk, M., Jaroniec, M., & Ryu, S. (1998). Characterization of structural and surface properties of activated carbon fibers. *Journal of Colloid and Interface Science, 204*(1), 151-156.

Lillo-Ródenas, M. A., Cazorla-Amorós, D., & Linares-Solano, A. (2003). Understanding chemical reactions between carbons and NaOH and KOH: An insight into the chemical activation mechanism. *Carbon, 41*(2), 267-275.

Lin, N., Huang, J., Chang, P. R., Feng, J., & Yu, J. (2011). Surface acetylation of cellulose nanocrystal and its reinforcing function in poly(lactic acid). *Carbohydrate Polymers, 83*(4), 1834-1842.

Liu, W., & Adanur, S. (2010). Properties of electrospun polyacrylonitrile membranes and chemically activated carbon nanofibers. *Text Res J. 80*(2),124-134.

Liu, Y., & Kumar, S. (2012). Recent progress in fabrication, structure, and properties of carbon fibers. *Polymer Reviews, 52*(3-4), 234-258.

Lordgooei, M., Carmichael, K. R., Kelly, T. W., Rood, M. J., & Larson, S. M. (1996). Activated carbon cloth adsorption-cryogenic system to recover toxic volatile organic compounds. *Gas Separation and Purification, 10*(2), 123-130.

Lozano-Castelló, D., Calo, J. M., Cazorla-Amorós, D., & Linares-Solano, A. (2007). Carbon activation with KOH as explored by temperature programmed techniques, and the effects of hydrogen. *Carbon, 45*(13), 2529-2536.

Lu, P., & Hsieh, Y. (2009). Cellulose nanocrystal-filled poly(acrylic acid) nanocomposite fibrous membranes. *Nanotechno, 20*(41), 415604.

Luo, J., Chang, H., Wang, P., Moon, R. J., & Kumar, S. (2018). Cellulose nanocrystals effect on the stabilization of polyacrylonitrile composite films. *Carbon, 134*, 92-102.

Maddah, B., Soltaninezhad, M., Adib, K., & Hasanzadeh, M. (2017). Activated carbon nanofiber produced from electrospun PAN nanofiber as a solid phase extraction sorbent for the preconcentration of organophosphorus pesticides. *Separation Science & Technology, 52*(4), 700-711.

Magalhães, F. D., Laurence, R. L., & Conner, W. C. (1998). Diffusion of cyclohexane and alkylcyclohexanes in silicalite. *The Journal of Physical Chemistry B, 102*(13), 2317-2324.

Maleknia, S. D., Bell, T. L., & Adams, M. A. (2007). PTR-MS analysis of reference and plant-emitted volatile organic compounds. *International Journal of Mass Spectrometry, 262*(3), 203-210.

Miao, J., Miyauchi, M., Simmons, T. J., Dordick, J. S., & Linhardt, R. J. (2010). Electrospinning of nanomaterials and applications in electronic components and devices. *Journal of Nanoscience and Nanotechnology. 10(9),* 5507-5519.

Mohamed, M. F., Kang, D., & Aneja, V. P. (2002). Volatile organic compounds in some urban locations in United States. *Chemosphere, 47*(8), 863-882.

Niu, H., Zhang, J., Xie, Z., Wang, X., & Lin, T. (2011). Preparation, structure and supercapacitance of bonded carbon nanofiber electrode materials. *Carbon, 49*(7), 2380-2388.

Nuraje, N., Khan, W. S., Lei, Y., Ceylan, M., & Asmatulu, R. (2013). Superhydrophobic electrospun nanofibers. *J. Mater. Chem. A., 1*(6),1929-1946.

Olsson, R. T., Fogelström, L., Martínez-Sanz, M., & Henriksson, M. (2011). Cellulose nanofillers for food packaging. *Multifunctional and nanoreinforced polymers for food packaging*, 86-107.

Orts, W., Shey, J., Imam, S., Glenn, G., Guttman, M., & Revol, J. (2005). Application of cellulose microfibrils in polymer nanocomposites. *Journal of Polymers and the Environment, 13*(4), 301-306.

Osmond, N. M. (2000). Activated carbon fibre adsorbent materials. *Adsorption Science & Technology, 18*(6), 529-539.

Otowa, T., Tanibata, R., & Itoh, M. (1993). Production and adsorption characteristics of MAXSORB: High-surface-area active carbon. *Gas Separation and Purification, 7*(4), 241-245.

Ouyang, Q., Cheng, L., Wang, H., & Li, K. (2008). Mechanism and kinetics of the stabilization reactions of itaconic acid-modified polyacrylonitrile. *Polymer Degradation and Stability, 93*(8), 1415-1421.

Park, W., Kang, M., Kim, H., & Jin, H. (2007). Electrospinning of poly (ethylene oxide) with bacterial cellulose whiskers. *Macromolecular Symposia, 249-250*(1), 289-294.

Pelekani, C., & Snoeyink, V. L. (1999). Competitive adsorption in natural water: Role of activated carbon pore size. *Water Research, 33*(5), 1209-1219.

Peresin, M. S., Habibi, Y., Zoppe, J. O., Pawlak, J. J., & Rojas, O. J. (2010). Nanofiber composites of polyvinyl alcohol and cellulose nanocrystals: Manufacture and characterization. *Biomacromolecules, 11*(3), 674-681.

Prasanth, R., Nageswaran, S., Thakur, V. K., & Ahn, J. (2014). Electrospinning of cellulose: Process and applications. *Nanocellulose polymer nanocomposites*, 311-340.

Pré, P., Delage, F., Faur-Brasquet, C., & Le Cloirec, P. (2002). Quantitative structure–activity relationships for the prediction of VOCs adsorption and desorption energies onto activated carbon. *Fuel Processing Technology, 77*, 345-351.

Qin, Y., Wang, Y., Wang, H., Gao, J., & Qu, Z. (2013). Effect of morphology and pore structure of SBA-15 on toluene dynamic adsorption/desorption performance. *Procedia Environmental Sciences, 18*, 366-71.

Ra, E. J., Kim, T. H., Yu, W. J., An, K. H., & Lee, Y. H. (2010). Ultramicropore formation in PAN/camphor-based carbon nanofiber paper.*Chemical Communications, 46*(8), 132-1322.

Raghavan, P., Lim, D., Ahn, J., Ahn, H., Nah, C., Sherrington, D. C., & Ryu, H. (2012). Electrospun polymer nanofibers: The booming cutting edge technology. *Reactive and Functional Polymers, 72*(12), 915-930.

Rahaman, M., Chaki, T. K., & Khastgir, D. (2011). High performance EMI shielding materials based on short carbon fiber-filled ethylene vinyl acetate copolymer, acrylonitrile butadiene copolymer, and their blends. *Polymer Composites, 32*(11), 1790-1805.

Ramakrishna, S., Jose, R., Archana, P. S., Nair, A. S., Balamurugan, R., Venugopal, J., & Teo, W. E. (2010). Science and engineering of electrospun nanofibers for advances in clean energy, water filtration, and regenerative medicine. *Journal of Materials Science, 45*(23), 6283-6312.

Raymundo-Piñero, E., Azaïs, P., Cacciaguerra, T., Cazorla-Amorós, D., Linares-Solano, A., & Béguin, F. (2005). KOH and NaOH activation mechanisms of multiwalled carbon nanotubes with different structural organisation. *Carbon, 43*(4), 786-795.

Ribes, A., Carrera, G., Gallego, E., Roca, X., Berenguer, M., & Guardino, X. (2007). Development and validation of a method for air-quality and nuisance odors monitoring of volatile organic compounds using multi-sorbent adsorption and gas chromatography/mass spectrometry thermal desorption system. *Journal of Chromatography A, 1140*(1), 44-55.

Rosas, J. M., Bedia, J., Rodríguez-Mirasol, J., & Cordero, T. (2009). HEMP-derived activated carbon fibers by chemical activation with phosphoric acid. *Fuel, 88*(1), 19-26.

Rufford, T. E., Hulicova-Jurcakova, D., & Zhu, J. Y. (2013). *Green carbon materials: Advances and applications*. Boca Raton, FL: CRC Press.

Ryu, Z., Rong, H., Zheng, J., Wang, M., & Zhang, B. (2002). Microstructure and chemical analysis of PAN-based activated carbon fibers prepared by different activation methods. *Carbon, 40*(7), 1144-1147.

Saha, D., & Grappe, H. A. (2017). In Chen J. Y. (Ed.), *5 - adsorption properties of activated carbon fibers*. Oxford: Woodhead Publishing.

Samir, M., Alloin, F., & Dufresne, A. (2005). Review of recent research into cellulosic whiskers, their properties and their application in nanocomposite field. *Biomacromolecules, 6*(2), 612-626.

Sánchez-Montero, M. J., Salvador, F., & Izquierdo, C. (2008). Reactivity and porosity of a carbon fiber activated with supercritical CO2. *The Journal of Physical Chemistry C., 112*(13),4991-4999.

Sánchez-Soto, P. J., Avilés, M. A., del Río, J. C., Ginés, J. M., Pascual, J., & Pérez-Rodríguez, J. L. (2001). Thermal study of the effect of several solvents on polymerization of acrylonitrile and their subsequent pyrolysis. *Journal of Analytical and Applied Pyrolysis, 58*, 155-172.

Scholten, E., Bromberg, L., Rutledge, G. C., & Hatton, T. A. (2011). Electrospun polyurethane fibers for absorption of volatile organic compounds from air. *ACS Applied Materials and Interfaces, 3*(10), 3902-3909.

Shen, W., Li, Z., & Liu, Y. (2010). Surface chemical functional groups modification of porous carbon. *Recent Patents on Chemical Engineering, 1*(1), 27-40.

Shonnard, D. R., & Hiew, D. S. (2000). Comparative environmental assessments of VOC recovery and recycle design alternatives for a gaseous waste stream. *Environmental Science & Technology, 34*(24), 5222-5228.

Sill, Travis J.|von Recum, Horst A. (2008). Electrospinning: Applications in drug delivery and tissue engineering. *Biomaterials, 29*(13), 1989-2006.

Siqueira, G., Bras, J., & Dufresne, A. (2009). Cellulose whiskers versus microfibrils: Influence of the nature of the nanoparticle and its surface functionalization on the thermal and mechanical properties of nanocomposites. *Biomacromolecules, 10*(2), 425-432.

Siró, I., & Plackett, D. (2010). Microfibrillated cellulose and new nanocomposite materials: A review. *Cellulose, 17*(3), 459-494.

Song, X., wang, Z., li, Z., wang, C., (2008). Ultrafine porous carbon fibers for SO2 adsorption via electrospinning of polyacrylonitrile solution. *Journal of colloid and interface science, 327*, 388–392.

Song, Y., Qiao, W., Yoon, S., Mochida, I., Guo, Q., & Liu, L. (2007). Removal of formaldehyde at low concentration using various activated carbon fibers. *Journal of Applied Polymer Science, 106*(4), 2151-2157.

Sturcová, A., Davies, G. R., & Eichhorn, S. J. (2005). Elastic modulus and stress-transfer properties of tunicate cellulose whiskers. *Biomacromolecules, 6*(2), 1055-1061.

Sullivan, P., Moate, J., Stone, B., Atkinson, J., Hashisho, Z., & Rood, M. (2012). Physical and chemical properties of PAN-derived electrospun activated carbon nanofibers and their potential for use as an adsorbent for toxic industrial chemicals. *Adsorption, 18*(3), 265-274.

Suzuki, M. (1994). *Activated carbon fiber: Fundamentals and applications*

Tang, M. M., & Bacon, R. (1964). Carbonization of cellulose fibers—I. low temperature pyrolysis. *Carbon, 2*(3),211-220.

Tashiro, K., & Kobayashi, M. (1991). Theoretical evaluation of three-dimensional elastic constants of native and regenerated celluloses: Role of hydrogen bonds. *Polymer, 32*(8), 1516-1526.

Treybal, R. E., 1915. (1980). *Mass-transfer operations*. United States.

Tsai, J., Chiang, H., Chiang, H., & Huang, G. (2008). Adsorption characteristics of acetone, chloroform and acetonitrile on sludge-derived adsorbent, commercial granular activated carbon and activated carbon fibers. *Journal of Hazardous Materials, 154*(1), 1183-1191.

Wang, G., Dou, B., Zhang, Z., Wang, J., Liu, H., & Hao, Z. (2015). Adsorption of benzene, cyclohexane and hexane on ordered mesoporous carbon. *Journal of Environmental Sciences, 30*(4), 65-73.

Wang, G. S., Kim, C., Jae Wook, L. E. E., Je Jung, Y. U. N., Jeong, Y. I., Moon, H., & Kap, S. Y. (2006). Adsorption characteristics of benzene on electrospun-derived porous carbon nanofibers. *Journal of Applied Polymer Science,* (3), 2454.

Wang, J., & Lin, Y. (2008). Functionalized carbon nanotubes and nanofibers for biosensing applications. *Trends in Analytical Chemistry, 27*(7), 619-626.

Wang, P. H., Yue, Z. R., & Liu, J. (1996). Conversion of polyacrylonitrile fibers to activated carbon fibers: Effect of activation. *Journal of Applied Polymer Science, 60*(7), 923-929.

Wang, T., & Kumar, S. (2006). Electrospinning of polyacrylonitrile nanofibers. *Journal of Applied Polymer Science, 102*(2), 1023-1029.

Weast, R. C.*CRC handbook of chemistry and physics*. Boca Raton, Fla: CRC-Press; 1984. p. C154–321

Wu, Q., Henriksson, M., Liu, X., & Berglund, L. A. (2007). A high strength nanocomposite based on microcrystalline cellulose and polyurethane. *Journal of Applied Polymer Science, 33*(8), 2877-2884.Xue, R., Yan, J., Liu, X., Tian, Y., & Yi, B. (2011). Effect of activation on the carbon fibers from phenol–formaldehyde resins for electrochemical supercapacitors. *Journal of Applied Electrochemistry, 41*(11), 1357-1366.

Yang, R. T. (1987). *Gas separation by adsorption processes*. Boston: Butterworths.

Yang, X., Wan, Y., Zheng, Y., He, F., Yu, Z., Huang, J., Gao, B. (2019). Surface functional groups of carbon-based adsorbents and their roles in the removal of heavy metals from aqueous solutions: A critical review. *Chemical Engineering Journal, 366*, 608-621.

Yue, Z., & Economy, J. (2017). 4 - carbonization and activation for production of activated carbon fibers. In J. Y. Chen (Ed.), *Activated carbon fiber and textiles* (pp. 61-139). Oxford: Woodhead Publishing.

Zaher Hashisho, Mark Rood, & Leon Botich. (2005). Microwave-swing adsorption to capture and recover vapors from air streams with activated carbon fiber cloth. *Environmental Science & Technology, 39*(17), 6851-6859.

Zhang, X. (2010). Fabrication of carbon nanofiber-driven electrodes from electrospun polyacrylonitrile/polypyrrole bicomponents for high-performance rechargeable lithium-ion batteries. *Journal of Power Sources, 195*(7), 2050-2056.

Zhang, X., Gao, B., Creamer, A. E., Cao, C., & Li, Y. (2017). Adsorption of VOCs onto engineered carbon materials: A review. *Journal of Hazardous Materials, 338*, 102-123.

Zhang, Z., Wu, Q., Song, K., Ren, S., Lei, T., & Zhang, Q. (2015). Using cellulose nanocrystals as a sustainable additive to enhance hydrophilicity, mechanical and thermal properties of poly (vinylidene fluoride)/poly(methyl methacrylate) blend. *ACS Sustainable Chemistry & Engineering, 3*(4), 574-582.

Zhou, C., Chu, R., Wu, R., & Wu, Q. (2011). Electrospun polyethylene oxide/cellulose nanocrystal composite nanofibrous mats with homogeneous and heterogeneous microstructures. *Biomacromolecules, 12*(7), 2617-2625.

Zussman, E., Chen, X., Ding, W., Calabri, L., Dikin, D. A., Quintana, J. P., & Ruoff, R. S. (2005). Mechanical and structural characterization of electrospun PAN-derived carbon nanofibers. *Carbon, 43*(10), 2175-2185.

Appendices

Appendix A: MEK adsorption data

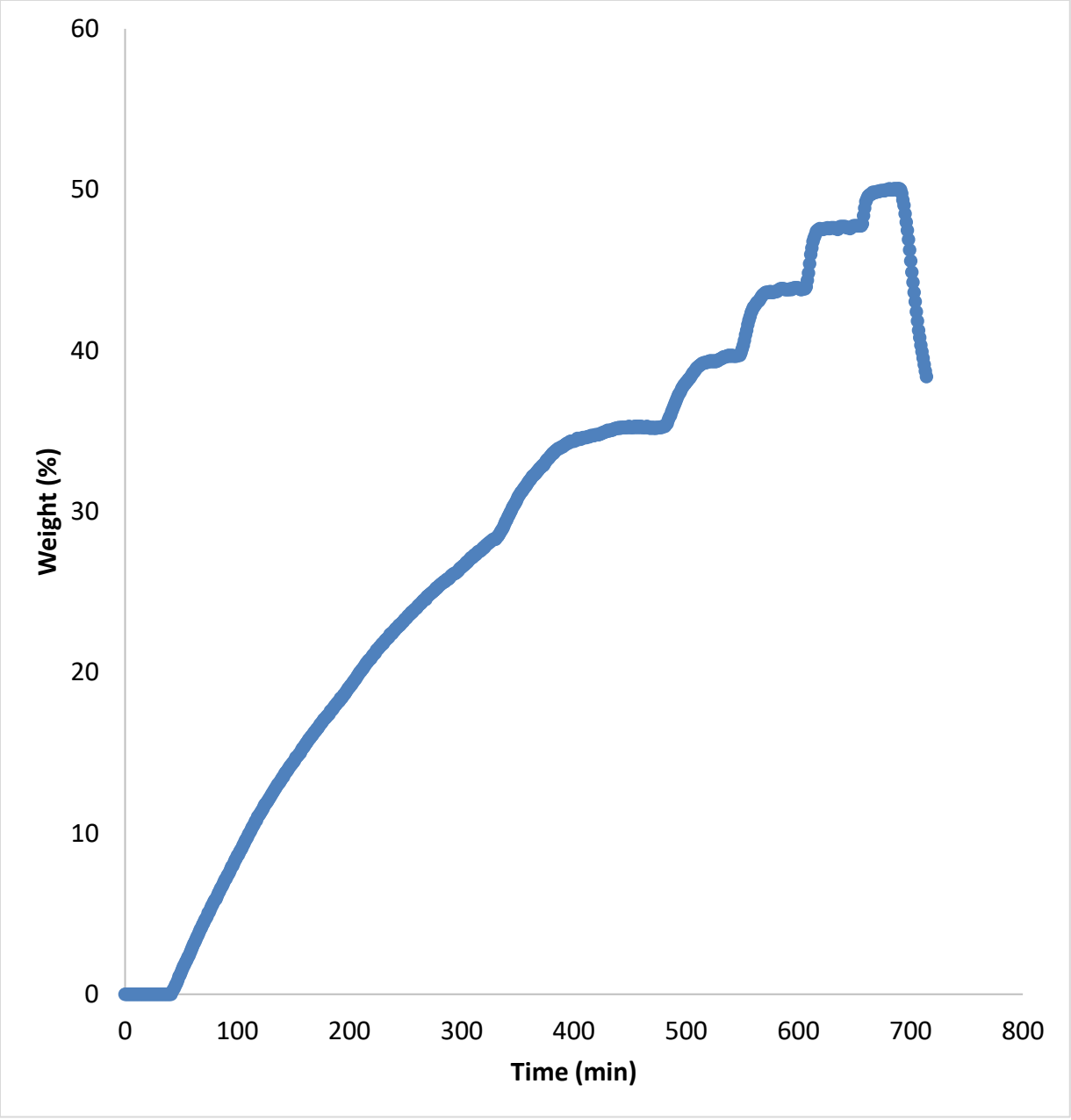

Figure A. 1 Adsorption data for MEK on 10%PAN only ACnF

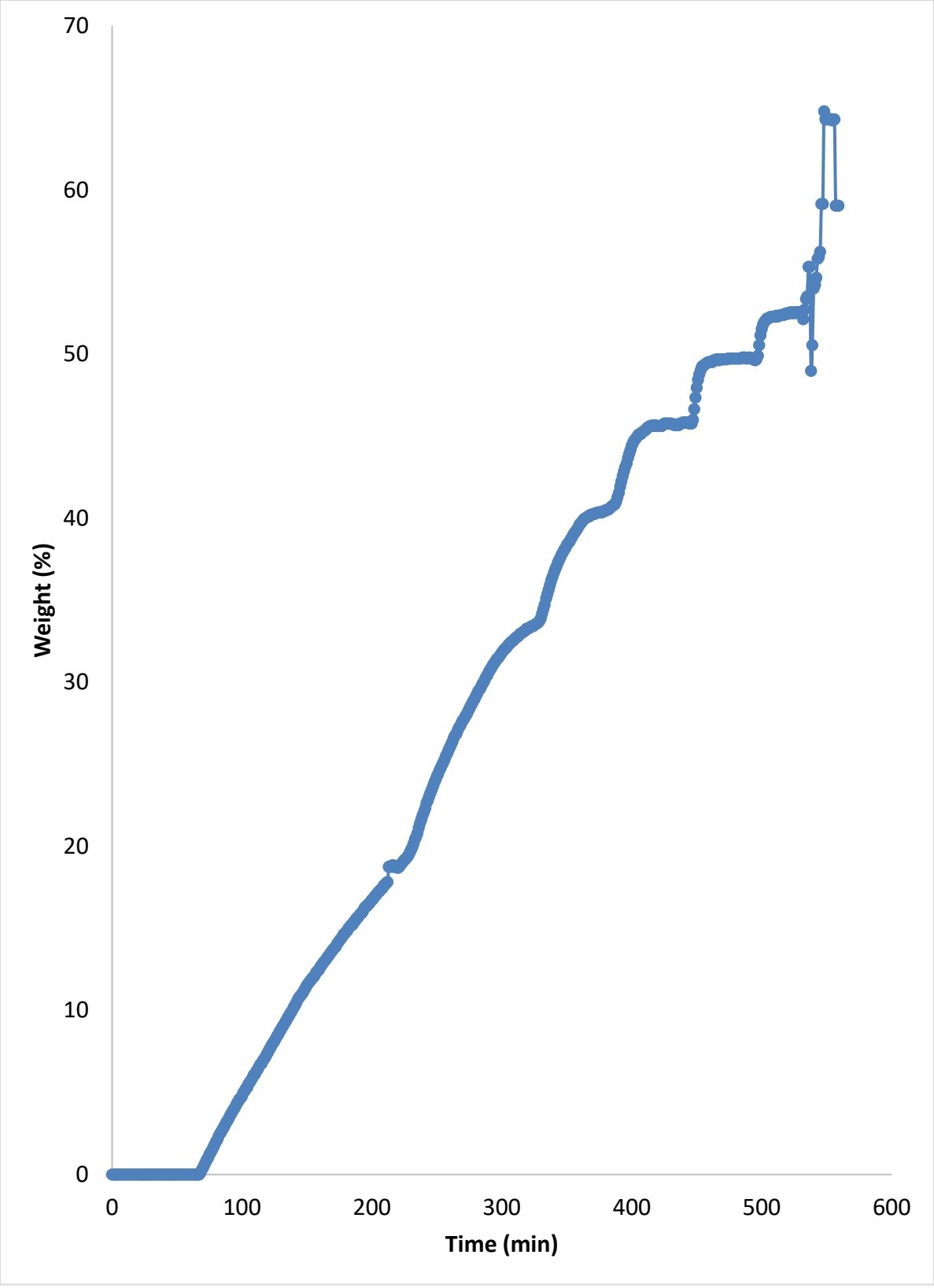

Figure A. 2 Adsorption data for MEK on 10%PAN-10%CNC ACnF

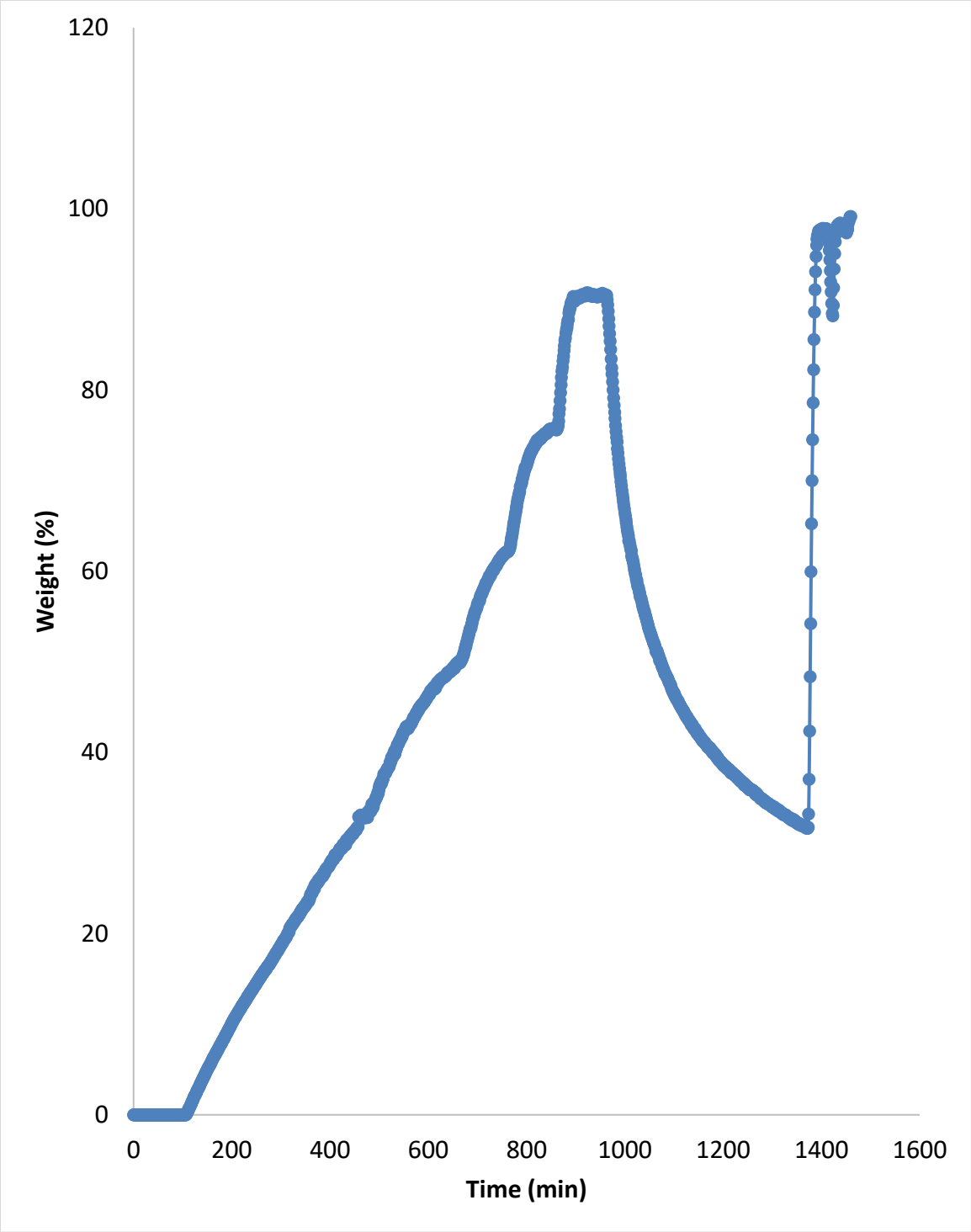

Figure A. 3 Adsorption data for MEK on 10%PAN-20%CNC ACnF

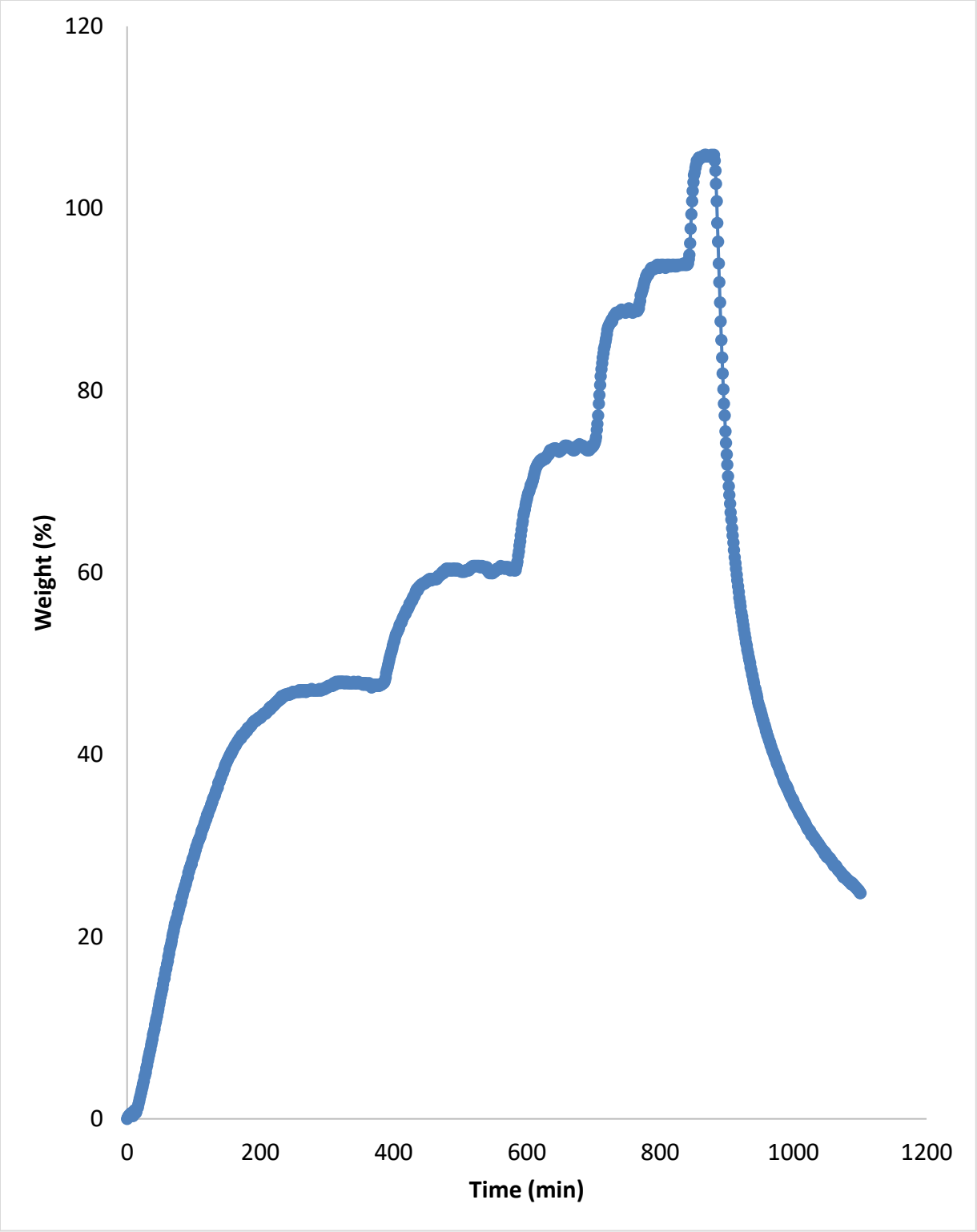

Figure A. 4 Adsorption data for MEK on 10%PAN-30%CNC ACnF

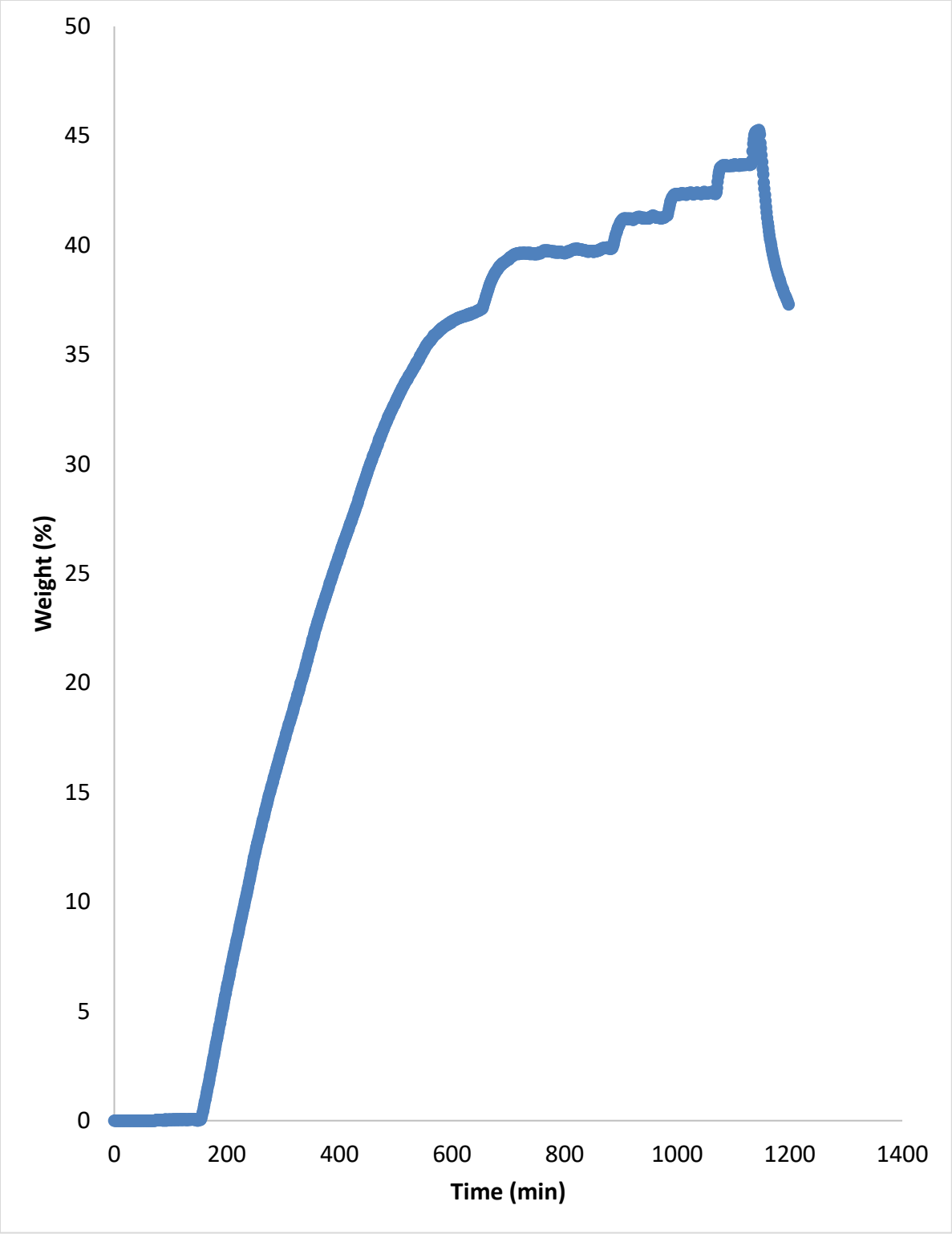

Figure A. 5 Adsorption data for MEK on ACFC-15

Appendix B: Cyclohexane adsorption data

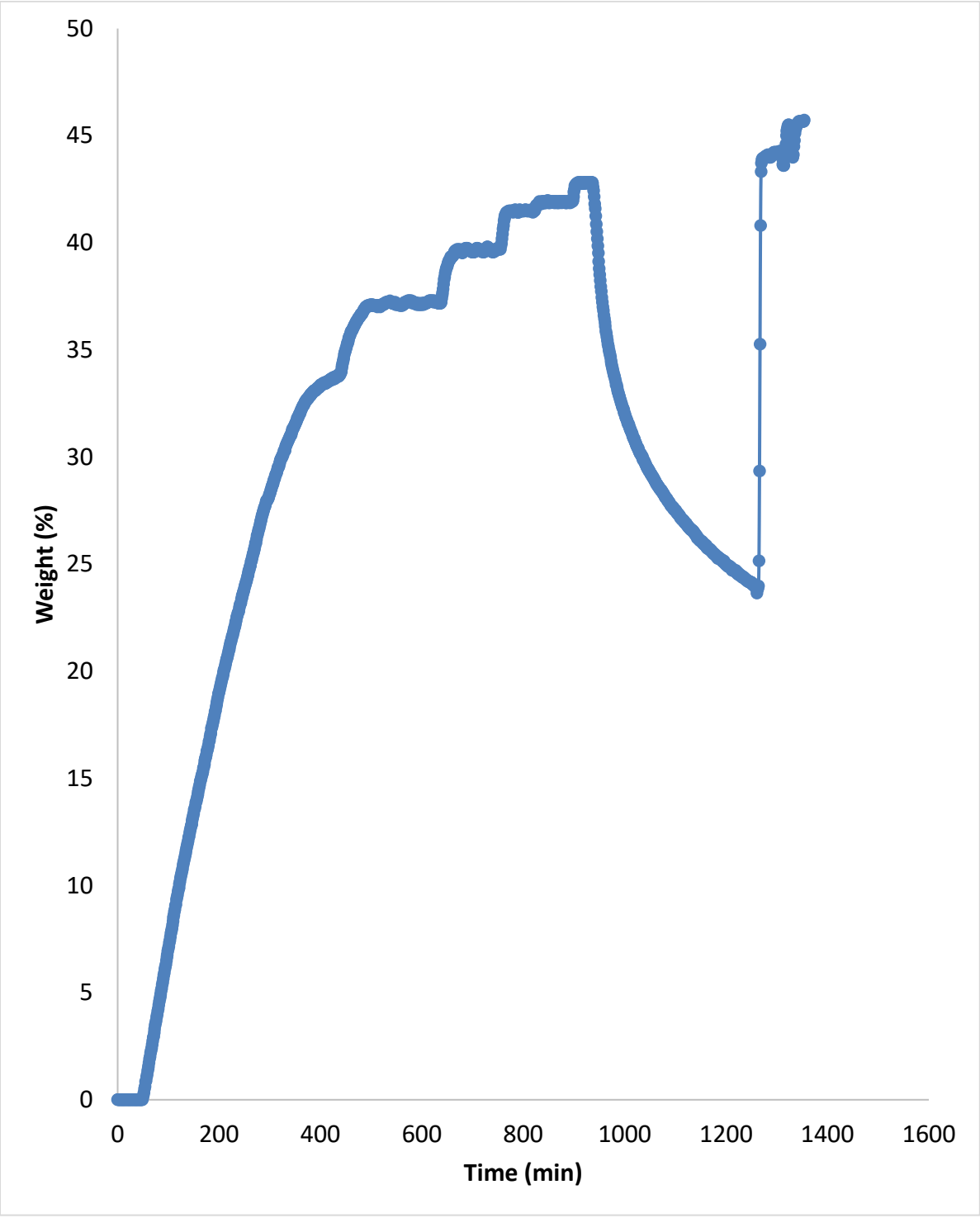

Figure B. 1 Adsorption data for cyclohexane on 10%PAN ACnF

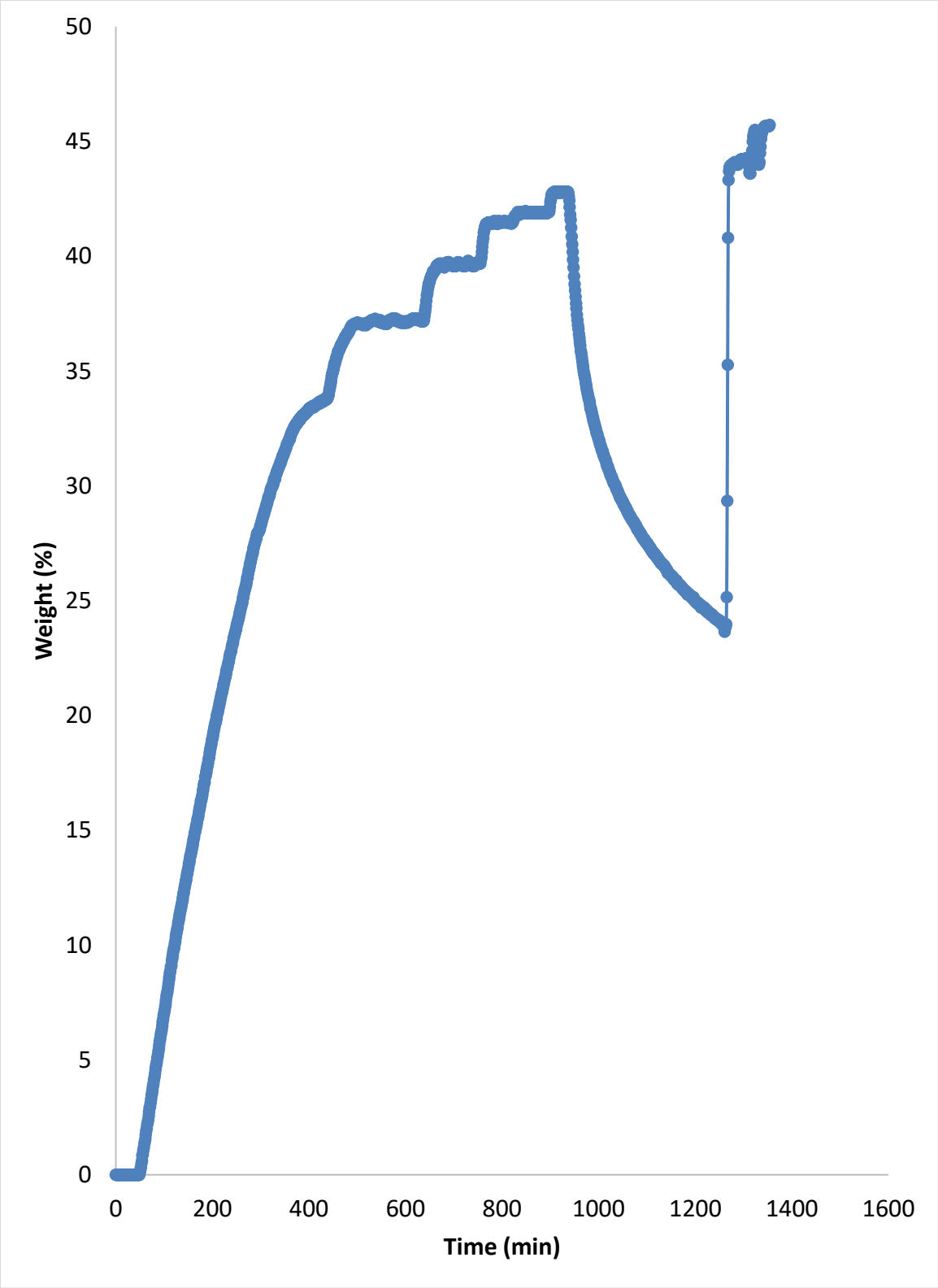

Figure B. 2 Adsorption data for cyclohexane on 10%PAN-10%CNC ACnF

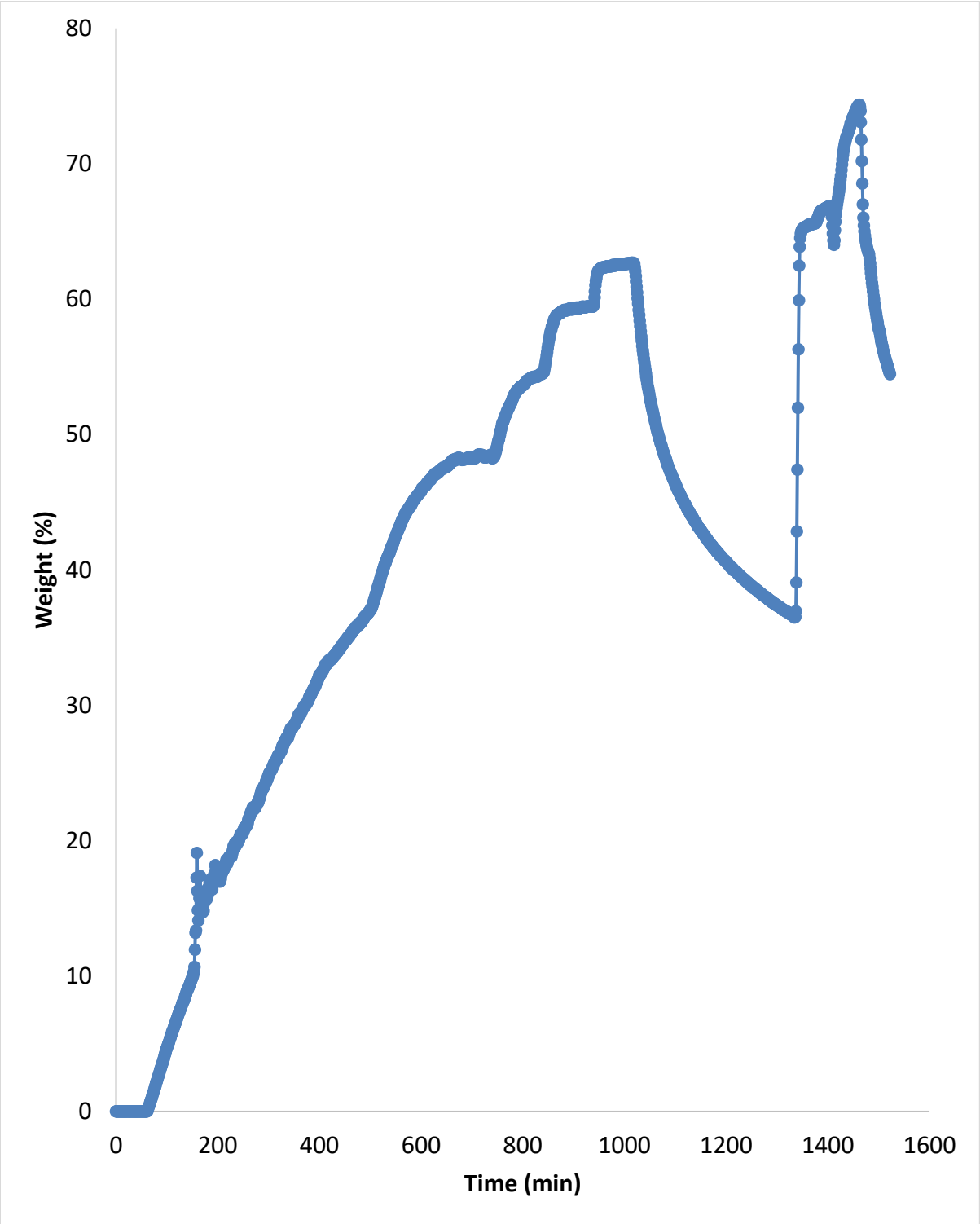

Figure B. 3 Adsorption data for cyclohexane on 10%PAN-20%CNC ACnF

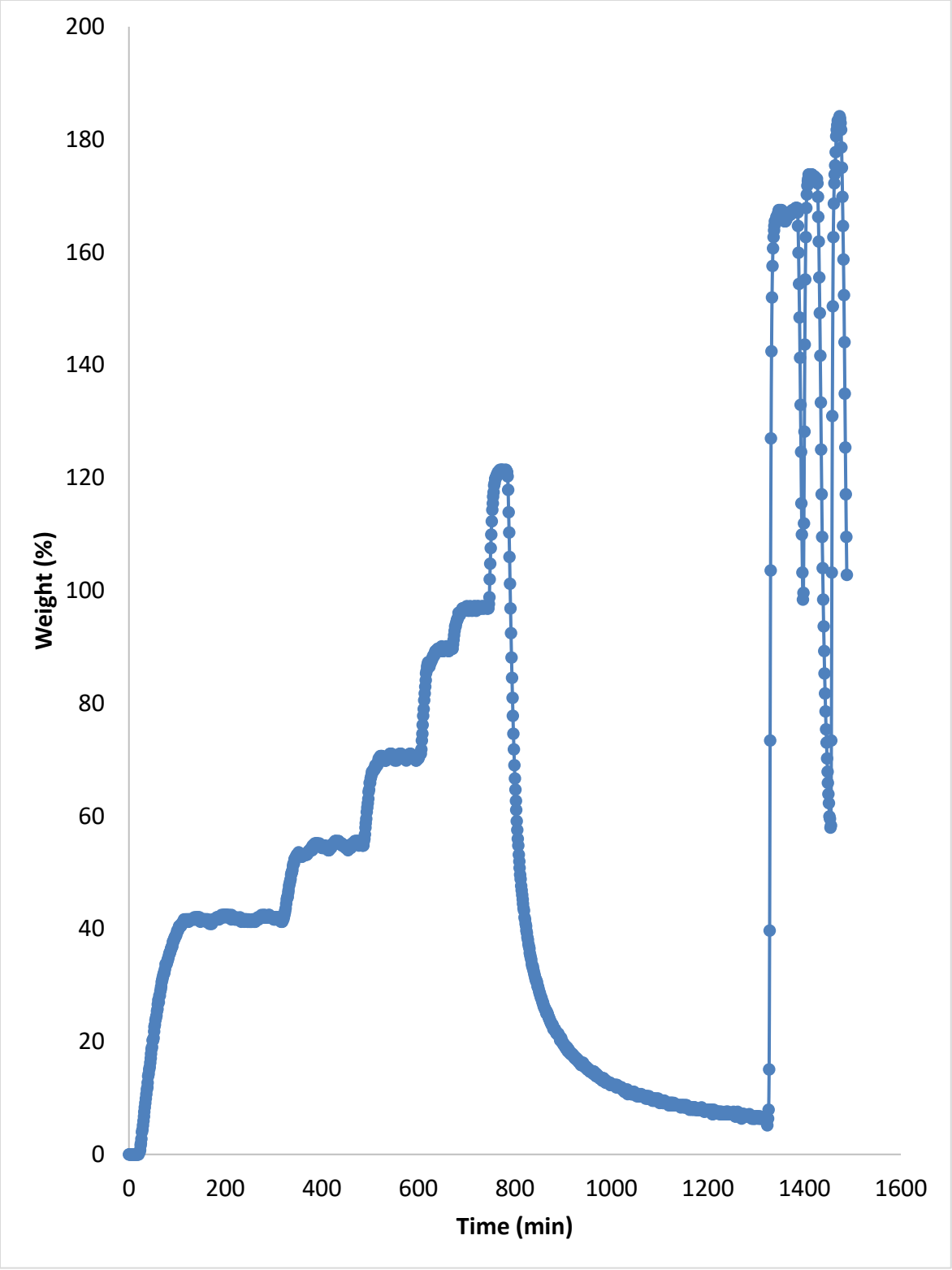

Figure B. 4 Adsorption data for cyclohexane on 10%PAN-30%CNC ACnF

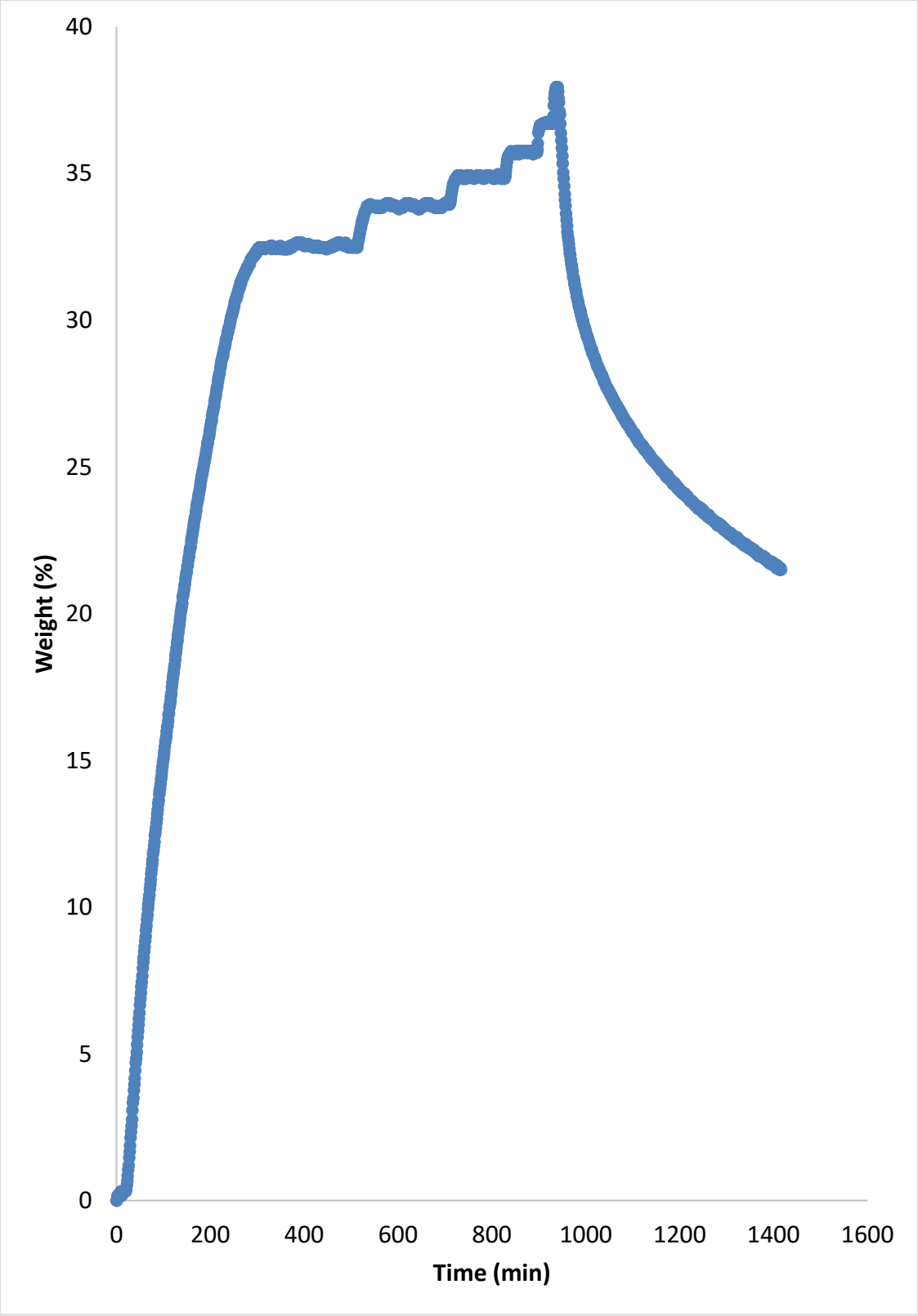

Figure B. 5 Adsorption data for cyclohexane on ACFC-15